The mineral-PET rock sorter: a study of the (γ,n) activation process

S M Phoku

Mini-dissertation submitted in partial fulfillment of the requirements for the degree of Masters of science in Applied Radiation Science and Technology at the Mafikeng Campus of the North-West University

Supervisors: Prof S H Connell
: Mr S Ballestrero

Sep 2014

DECLARATION

This dissertation reports original reseach carried out at iThemba Laboratory for Accelerator Based Sciences (iThemba LABS) in collaboration with the Centre for Applied Radiation Science and Technology (CARST) at the North-West University (Mafikeng Campus).

I hereby declare that the work contained in this dissertation is my own work and has not been submitted for any degree or examination at any other University or Institution.

Signed:_____ Date:_____

Samuel Marothi Phoku

Abstract

Positron Emission Tomography is a technique used for imaging in diagnostic medicine. In this technique a nutrient is labeled with a positron emitter and imaging of the metabolic uptake rates is performed. Mineral-PET uses an analogous process where a diamond inside a kimberlite rock can be imaged in an on-line mining situation.

The diamond is PET-inactive and therefore a minute fraction of carbon atoms need to be temporarily activated as a positron radiation source. Gamma radiation is used to convert the dominant carbon-12 isotope to the positron emitter isotope carbon-11, via the gamma-neutron (γ,n) nuclear reaction. The emitted positron thermalizes and annihilates with an electron resulting in two back-to-back gamma photons, each at 511 keV energy, which is then detected by the matrix of position sensitive fast timing BGO (bismuth germanate - $Bi_{12}Ge_4O_4$) detectors.

This study investigate the activation process where gamma photons in the energy range of around 25 MeV are produced by bremsstrahlung from an electron beam, where a high atomic number material is used as a target. The study then concludes on the parameters of accelerator design (i.e. converter type and thickness and electron beam energy) based on the feasibility study of the new technology.

Acknowledgement

I would like to acknowledge the following people:
Mr. S. Ballestrero and Prof. S.H. Connell for dedicating their time to helping me in my academic and professional development. This dissertation could never have been possible without their supervision.

My family for their support, understanding and giving me a chance to pursue my studies. They continued to support me financially and morally even when it was my turn to return the favour.

Welly Mampe, Thomas Sibiya, Lucky Mkhonza, Mark Dalton, Georgy Mbianda, Winile Sibande, all people at iThemba LABS and Wits school of physics I worked with. They have contributed in assisting me technically and in adding knowledge. They were always available when I needed help. A special thanks Dr Morgan Madhuku, who has always encouraged me and was always interested in my progress.

iThemba Laboratory for Accelerator Based Sciences (iThemba LABS), South African Nuclear Nuclear Cooperation (NECSA), WITS University, University of North-West (Centre for Applied Radiation Science Technology) for letting me use their resources and contributing to my development.

The National Research Foundation (NRF), Bateman Minerals, and CARST for supporting my studies financially.

Contents

List of Figures

List of Tables

List of Abbreviations

BGO	Bismuth Germanate
FWHM	Full-With at Half Maximum
FWTM	Full Width at Tenth Maximum
GDR	Giant Dipole Resonance
LINAC	Linear Accelerator
LSO	Lutetium Orthosilicate
PET	Positron Emission Tomography
Z	Atomic number

Chapter 1

Introduction

1.1 The Mineral-PET diamond-ore sorting system

The diamond mining and processing industry is one of the fastest growing and developing industries in South Africa and the world. The mining and processing methods are developing and advancing to become more time and cost efficient. One of the ways of extracting diamond is described by Ballestrero *et al.,* (2009) where the large rocks from diamond mining are initially reduced in size, by means of a crusher with counter-rotating cylinders, to particles of approximately 10 - 15 cm, using water both to cool the system and to contain volatile dust. This "first crush" is then further crushed down to a size of a few millimetres. It is then assumed that in this "final crush" the diamonds are going to be exposed on the surface, and one of two techniques is used: either the traditional grease table, or X-ray absorption (Meyer, 1988). Only a minute fraction of the first crush actually contains any significant diamond particles, and in practice most of the energy, water and machinery are wasted on processing barren material. Alternative to this method is the proposed Mineral-PET (Positron emission Tomography), a new method under study which is intended to improve the diamond mining process.

The Mineral-PET diamond-ore sorting system is being developed for mining applications in sorting diamondiferous rocks from barren ones. There are two major steps in the Mineral-PET project: the activation and the detection processes.

Activation is a process where the possible diamond bearing kimberlite rocks are bombarded with bremsstrahlung photons in order to make them radioactive. The (γ,n) nuclear reaction is induced in the kimberlite rock, and as a result the carbon-12 in the diamond and in the rock is transmuted to radioactive carbon-11. The carbon-11 emits positrons when it decays, and it is termed a β^+ emitter. These positrons can react with free electrons and annihilate to two back-to-back γ photons, each of 511 keV energy which can be detected using PET detectors.

In the detection process, PET/γ radiation detectors are used to detect the presence of diamond inside the kimberlite. These detectors must be placed opposite to each other so that the two back-to-back photons from positron annihilation resulting from activation can fall on to them and be detected. An array of detectors is used to improve the detection probability since the annihilation can be in any direction in a 360^o volume. An overview of the Mineral-PET system is illustrated in Figure 1.1.

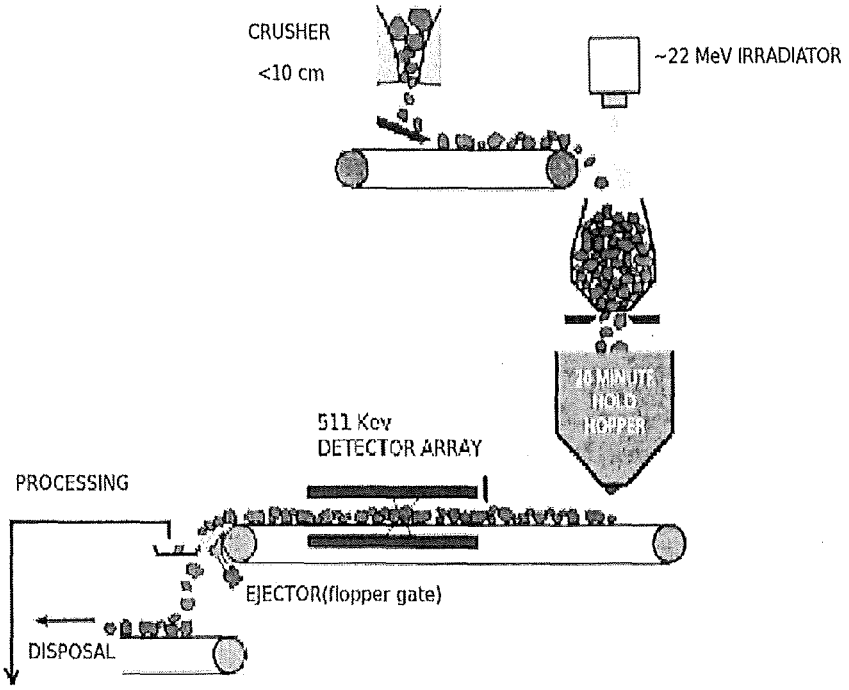

Figure 1.1: The overview of Mineral-PET process

This research addresses the activation process of kimberlite rock using bremsstrahlung photons and also the detection efficiency of the detector system in Mineral-PET. It consequently addresses the feasibility of the method in terms of the physics, economic viability, applicability, and the quality of the diamond extracted by this method.

1.2 Aim of research

The aim of this research is to optimize the accelerator parameters for the activation of kimberlite. The investigated parameters are: 1) the type and thickness of the converter material. The converter material is used to convert the electron flux into bremsstrahlung which activates the kimberlite material (including the possible diamond insert) when it interact with it in a photo-nuclear reaction. 2) the beam energy (E) and current (I) which are the specifications on the accelerator design.

1.3 Thesis outline

This chapter summarizes the whole research project, and clarifies the goals in the activation calculations and processes. It also explains the detection of photons on PET detectors, where the interaction of photons with the detector is looked at.

Chapter two explains the theoretical aspects of the study, whereby the Medical-PET and the feasibility study of Mineral-PET are reviewed. Here the physics that goes into the functioning of the project, the environment in which the project will operate and also the estimated costs of getting the project running are explained. It also explains briefly how the environment and the people who will be involved in the Mineral-PET project will be protected from radiation. In the Medical-PET, the physics is reviewed. This physics is similar to that of Mineral-PET, in fact Mineral-PET was developed from Medical-PET by the Late Prof. JPF Sellschop (Sellschop & Conell, 2005). Medical-PET will be compared with Mineral-PET by looking at the difference in the algorithms and detection methods between the two PET processes.

Chapter three looks at the calculation of the activation parameters so as to conclude on the flux of electrons and hence the accelerator current. How much of the diamond is activated is also looked at in order to assure that the quality of the diamond will not be affected.

In chapter four the Monte Carlo simulation of photon production using an electron beam of varying energies (in the order of MeV), targeting materials of high atomic number and of various material types and thicknesses is explained. These materials are used for the production of bremsstrahlung photons by converting electron energy into γ energy and they are referred to as converters in this project. The converted γ photons are then used in the activation of the kimberlite rocks and this activation occurs at a specific energy region or

cross-section. Therefore the cross-section of the activation and also of the entire γ spectrum during the process of activation will be shown. The chapter will concentrate specifically on the cross-section in the region of the desired γ spectrum. All this is done to optimize the design parameters of the accelerator which will be used for the production of activation γ's.

Chapter five gives the results and the analysis for simulations of the optimization of accelerator parameters. The measurements of the experimental and the simulation results are compared. How the Mineral-PET can surpass the medical facility and gives better results at low activation radiation is also shown.

Chapter six briefly explains the experimental procedure which was done at the Karolinska medical facility in Sweden and shows how the background interference is suppressed with time delay, a situation similar to a hold Hooper in the actual operation of Mineral-PET. This experiment verifies the results of the Monte Carlo simulation. A comparison between Mineral-PET facility and the Medical-PET facility can also be seen here.

Chapter seven draws conclusions on the simulation and expected results by looking at the global efficiency of the Mineral-PET, the efficiency of the activation bremsstrahlung material, and the detector efficiency. In general, conclusions on the optimum parameters of accelerator design are made.

1.4 Producing electron bremsstrahlung in the energy range of 22 to 27 MeV

This research project is fundamentally based on the production of bremsstrahlung photons in the energy range of 22 to 27 MeV, which is further discussed in section 2.2.2. When an electron of some energy E is incident on an atom and is able to penetrate the atom, it experiences some accelerating force from the electric field of the nucleus and the surrounding electrons of that atom. In order to conserve momentum when its velocity changes, it loses some energy in the form of photons. These photons are called bremsstrahlung. Photon emission depends on the electric field strength that is experienced by the electron (Leo, 1994). Thus, the bigger the atomic number (Z) the greater the amount of photons produced.

Materials of high Z and density (ρ) such as copper (Cu) and tungsten (W) are used as targets in bremsstrahlung photons production. When these materials are bombarded with high energy electrons they produce photons at high energies. These high energy photons can be used in a photo-nuclear activation reaction (Eshwarappaa *et al.,* 2007).

The electron-material interaction does not lead to production of high energy photons only. Other reactions which result are low energy photons such as Compton photons, but are not of interest in this project (See Figure 1.2).

1.5 Photon interactions with matter

The second part of the Mineral-PET system is the use of high energy photons in the activation of PET isotopes. When the PET isotopes release the annihilated photons (511 keV) they will be detected by an array of detectors arranged opposite to each other.

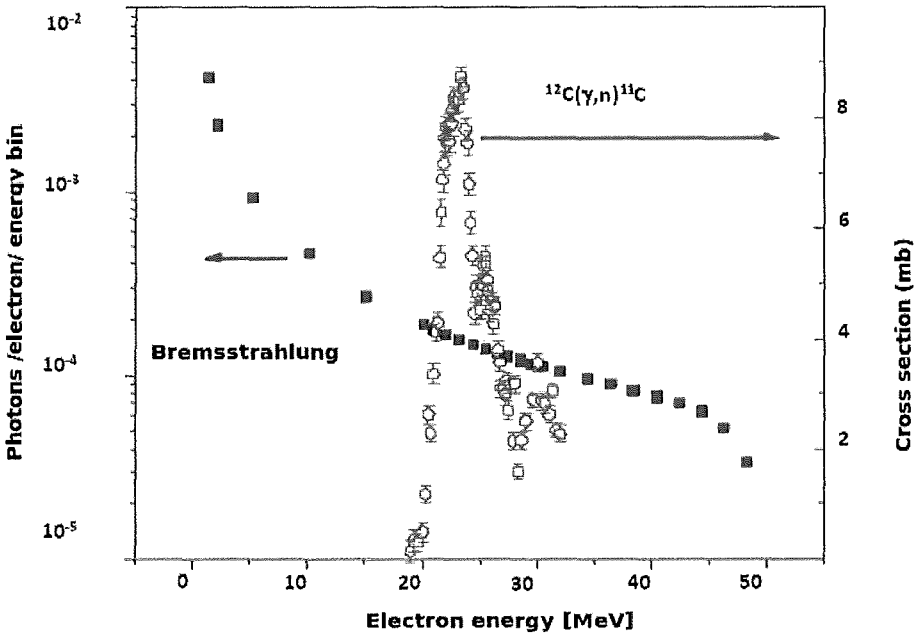

Figure 1.2: The production of bremsstrahlung photons from electron using a 1.3 mm tungsten target bombarded by a 50 MeV electron beam. The red insert shows the region of the (γ,n) resonance reaction for the production of the carbon PET isotope with a relatively large cross section of 8 mb. The picture is adapted from (Ballestrero *et al.*, 2005)

The interaction of photons with the detector material may occur in three ways, namely, Compton scattering, photoelectric absorption, and pair production. In Compton scattering, the incident photon collides with a bound electron of an atom and transfers some fraction of its energy to the electron. The electron gains some momentum and scatters at an angle relative to the fraction of the photon that is proceeding through the material. The angle of scatter varies between 0^o and 180^o and it can be a back scatter or a forward scatter. Thus the energy of the resulting photon and the transferred energy depend on the angle of scatter. A back scatter at 180^o will mean the maximum energy has been transferred to the electron, whereas a straight forward scatter at 0^o will mean a minimum energy has been transferred to the electron (Krane, 1988; Farr & Allisy Roberts, 2006).

In the photoelectric effect the total energy of the incident photon is transferred to the bound

electron. If the energy transferred is larger than the binding energy of the electron, the electron will be ejected from its orbital. The following equation expresses the photoelectric effect

$$E_T = E_p - E_b$$

where E_T is the total energy in the electron, E_p is the energy of the incident photon, and E_b is the binding energy of the electron. For an electron to be ejected E_b must be less than E_p (Farr & Allisy Roberts, 2006).

For pair production to occur the energy of the incident photon should be 1.022 MeV or more. In this interaction the photon is transformed into a positron-electron pair (Krane, 1988). The positron may later annihilate with an electron, usually not the same electron from pair production. The three processes are illustrated in Figure 1.3. (1) A photon scatters a few

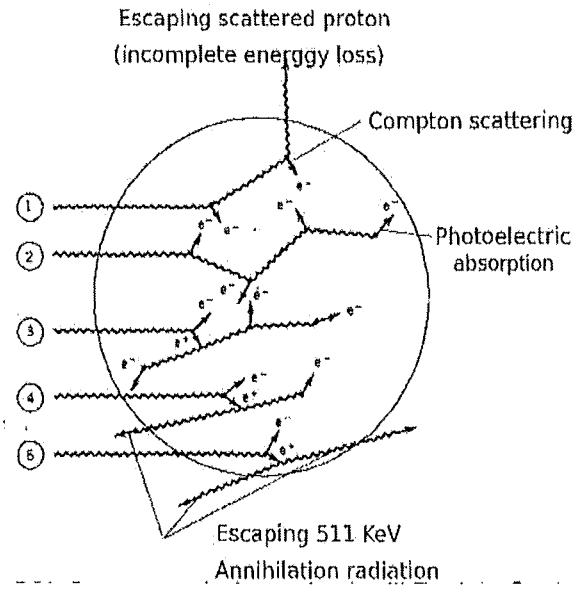

Figure 1.3: This Figure adopted from (Krane, 1988), shows the different interactions of photons with a detector.

times and then escapes from the detector without losing all of its energy (Compton scattering).

(2) There is a multiple Compton scattering and then a photoelectric effect. (3) It is a pair production (e^- and e^+) then followed by annihilation, Compton scattering, and photoelectric absorption respectively. (4) It is an annihilation where one of the photons escapes (this is called single escape) from the detector while the other is absorbed photoelectrically. (5) Here both the annihilation photons escape from the detector, and it is called double escape.

1.6 Scintillation process

A scintillator is a material which releases light when struck by a particle or a photon with a certain energy. This light released in the latter case carries energy proportional to that absorbed by the scintillator material. Therefore the more the energy absorbed the higher the intensity of the light.

Scintillation does not occur directly from photons interacting with the detector. It occurs when photons with a specific energy interact with the electrons of the detector material and excite them to promote them to a level higher in energy. When the excited electrons return to the ground state they lose their energy in the form of visible or near-visible light (Krane, 1988). The photons in a scintillator are visible light. The light signal is converted to an electronic signal which is amplified by an optically mounted photo-multiplier tube (PMT) and recorded as an electrical pulse, if this phenomenon is occurring in a detector system.

The PMT consist of, among others, photocathode, dynodes, and anode. The photocathode is on the side of the scintillator in the detector. When the photons from the scintillator strike on the photocathode, electrons are released by means of photoelectric effect. The electronic signal is amplified when the electrons from the cathode are transported to dynode through electric field. When the electrons from the cathode strike the dynode, the dynode releases more electrons to the next dynode. The dynodes are arranged in increasing voltages. The

multiplication of electrons continues until to the anode, when the signal is said to be amplified, and exit the PMT for further processing and recording.

1.7 Detector efficiency

The absolute detector efficiency is defined as events registered by the detector over the total events from the decay. The following factors are important: geometric efficiency, intrinsic efficiency, absorption and scatter and energy-selective counting. The geometry of the detector plays an important role in the sense that the surface of the detector receives the photons. Hence the total efficiency is a function of detector geometry and the probability of photon interaction in the detector. This probability depends on the cross-section of the incident photon on the detector material (Leo, 1994) and it is given by

$$P = 1 - e^{-\varepsilon_{tot}}$$

The Absolute efficiency is given by the product of geometrical efficiency and the intrinsic efficiency, mathematically expressed as

$$\varepsilon_{tot} = \varepsilon_{geo} \cdot \varepsilon_{int}$$

where ε_{geo} is the geometric efficiency, and ε_{int} is the intrinsic efficiency.

The geometric efficiency (ε_{geo}) depends on the source, the detector size and shape, and also on the distance between the detector and the source (inverse square law).

Intrinsic efficiency depends on the property of the detector material. This efficiency is defined as the number of events registered by the detector over events impinging on the detector, and

is expressed as

$$\varepsilon_{int} = 1 - e^{-\mu(E)x} \tag{1.1}$$

where $\mu(E)$ is the linear attenuation coefficient, and x is the thickness of the crystal. From equation 1.1 it can be seen that the term ε is proportional to $-\mu(E)x$ which is a function of energy of the photon. Table 1.1 provides a comparison of the relative efficiency of a NaI (sodium iodide) and a BGO (bismuth germanate) detector in terms of energy resolution and time response.

The next chapter explains how the interactions of photons and electrons with materials are fundamental to PET.

Table 1.1: Properties of a BGO detector compared to a NaI(Tl) detector

Material	Wavelength of max emission (nm)	Decay constant (μs)	Scintillation cut-off wavelength	Refractive index	Density (g/cm^3)	Hygro-scopic	Scintillation conversion efficiencies (%)
NaI(Tl)	415	0.23	320	1.85	3.69	yes	100
$Bi_4Ge_3O_{12}$	480	0.3	350	2.12	7.13	no	12

Chapter 2

Theoretical aspects of Mineral- and Medical-PET

2.1 Medical-PET

2.1.1 Introduction

Medical-PET (Positron Emission Tomography) is a diagnostic technique used in the medical application of radiation for functional imaging in human organs, whereby a biological nutrient is labeled with a positron emitting radionuclide (Pain *et al.*, 2008; Ollinger & Fessler, 1997; Daniel Ben, *et al.*, 2008). The nutrient undergoes a metabolic process in the selected organ. Therefore, the radio-labeled nutrient should be chosen in such a way that it is susceptible to the organ of interest. The metabolic functioning of an organ can then be imaged using an array of PET sensitive detectors. A typical array of PET detectors may be arranged in ring form and is normally called a PET scanner (Herzog, 2007; Krane, 1988; Ter-Pogossian & Phelps, 1975; Phelps, Hoffman & Mullani, 1975).

A gamma photon signal is formed when the positron emitted from the radionuclide combines with an electron and then they undergo annihilation. The electron usually does not come from the same nuclide. The annihilation results in two back-to-back photons which will fall onto two nearly opposite detectors in a ring. The annihilation can be three γ photons, but this is less likely to happen and has a 25% chance (Ballestrero *et al.*, 2009).

To detect dysfunctional organs there will be a high density of positron annihilations detected at a particular place compared to other places in the same organ related to the uptake rates of the nutrient. For example, cancer tissues grow faster and can consume more nutrients. The high density of γ rays would mean that there is no normal flow of the labeled nutrient and the consumption is also high. Among the radio-nuclides which can be used as positron emitters are ^{15}O, ^{13}N, ^{11}C, and ^{18}F which must be produced with a cyclotron next to the diagnostic facility because of their short half-lives, with ^{18}F being the longest (110 min) (Krane, 1988; Enge, 1970).

2.1.2 The basic physics principles in PET.

β emissions

The stability of isotopes depends on the ratio of protons and neutrons in the nucleus of an atom. If there are too many protons, proton rich or neutron deficient (Sorenson, Cherry & Phelps, 1987), in the atom so that it makes the atom unstable, then some of the protons will be converted to neutrons in order to reach the ratio of a stable atom. In the process fast positive electrons (positrons) and neutrons are produced (Krane, 1988; Knoll, 2000; Hake & Wolf, 1996; Cember, 1996). These electrons are called β^+ particles, and they originate from the nucleus (and not from the orbitals of the atom). The β^+ emission can be written as

$$p \rightarrow n + e^{+} + \nu_e$$

where the p is proton, n is neutron, e^{+} is positron, and ν_e is a neutrino. This process is termed β^{+} decay. Another particle called a neutrino is also emitted, but since it has no charge it does not influence the final nuclide being created.

A similar procedure occurs when the atom is neutron rich which makes the N/Z ratio to be high. The neutrons which are in excess will be converted to protons. In the process negative electrons, photons, and anti-neutrinos will be produced. This process is termed β^{-} decay. The corresponding equation will be

$$n \rightarrow p + e^{-} + \bar{\nu}_e$$

There is an alternative β decay in a proton-rich atom, where the nucleus with more protons than neutrons captures an electron from the nearby environment. The reaction is termed electron capture and it is as follows:

$$p + e^{-} \rightarrow n + \nu_e$$

The presence of anti-neutrinos or neutrinos is shown by a continuous energy on β particle spectrum. Figure 2.1 shows the decay momentum spectrum of β^{+} from carbon-11, showing a peak with maximum 386 keV spreading to an end point of 960 keV. The spread shows the presence of positrons which do not have a definite energy (Palmer & Parker, 2004; Wong, 1954).

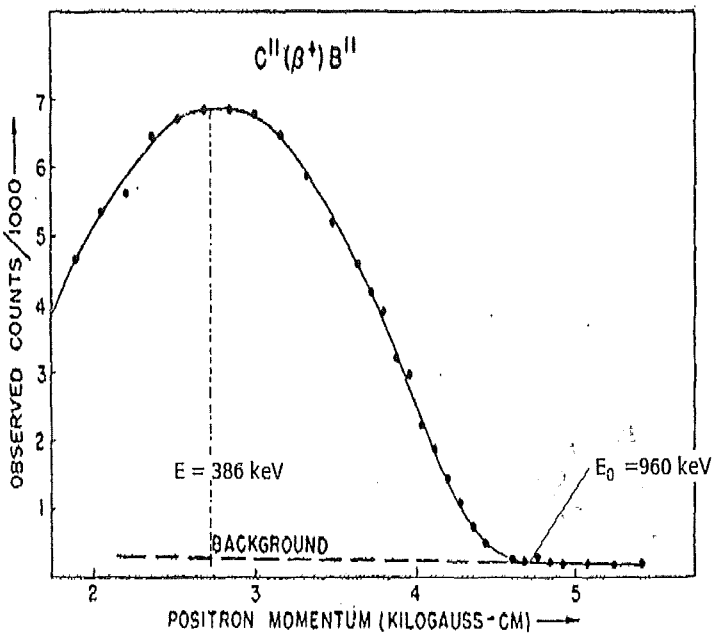

Figure 2.1: Carbon-11 positron decay spectrum (Wong, 1954)

Annihilation process

PET involves positron emission. When the positron is emitted it travels inside the material and loses its energy mostly through the Bethe-Bloch collision mechanism. It then combines with an electron of the same or another atom (Hendee, 1970; Sweet & Brownell, 1953; Price, 1967). The average distance it travels is different for different parent nuclides. Levin (1999) and Ballestrero *et al.,* (2009) have shown the distribution of distances between the decaying radionuclide and point of annihilation of a positron for different radionuclides modelled in water medium. The distribution generally has a sharp peak and a substantial tail. For carbon-11, the Full Width at Half Maximum (FWHM) and Full Width at Tenth Maximum (FWTM) of the distribution are 0.188 mm and 1.86 mm respectively. Using the Bethe-Bloch formula, which states that the probability of the positron in flight is inversely proportional to the velocity (Dirac, 1930), to scale from water to kimberlite, the distribution for the positron

range is 0.063 mm for FWHM and 0.63 mm for FWTM.

There are two possible reactions when an e^+ combines with an e^-. This depends on the total spin (S) of the system.

1. When S=0, there is direct annihilation to two γ rays in opposite directions. The two photons are released in such a way that the momentum of the system is conserved. Initially the two electrons (e^+ and e^-) have zero momentum. In order to conserve the momentum, the resultant annihilation photons are released back-to-back so that their velocities cancel each other. Each of the two photons has energy (511 keV) equivalent to the mass of the electron.

2. The other possible annihilation, when S=1, though with very small probability, is by first forming a state in which a positron and an electron form a light hydrogen-like atom called ortho-positronium bound by coulomb attraction forces. Followed by annihilation of three γ photons (Akhiezer & Berestetskii, 1965), whereas the positronium formed when S=0 is called para-positronium.

Interaction of γ photons with the detector material

There are three basic interactions of photons with matter, namely, the Compton scattering, the photoelectric effect, and pair production. Photons from annihilation (511 keV each) are too low in energy to cause pair production. Pair-production occurs for energies more than 1022 keV. Therefore, only the photoelectric effect and the Compton effect will be considered. In the photoelectric effect the photon loses all the energy to an electron which will be ejected from the atom due to the increased energy, while in the Compton effect only a fraction of the energy is transferred to the electron. The Compton effect is undesirable since it causes the deterioration of image resolution when the Compton photon energy deposition is scattered and

may escape the detector (Leo, 1994). BGO has a high photon stoping power and, therefore, it keeps this effect at minimal.

2.1.3 PET Detectors

In most cases, medical-PET uses scintillator detectors for imaging. This kind of detector basically consists of a scintillator which is a crystal, organic or inorganic liquid, plastic, etc. BGO is one of the detectors that is widely used in PET (Lecog, 1998). A scintillator detector emits light when it interacts with ionizing radiation, when the light reaches the photo-multiplier tube it is converted to an electrical output and then amplified. This signal can further be processed by amplifiers, analogue to digital converter (ADC) and computer programmes to turn it into a viewable image (Hamamatsu Photonics, 2001).

When a photon γ interacts with a scintillator it ionizes the scintillator atoms and in reaction to this ionization (i.e. neutralization of ions) the scintillator material loses energy by emitting visible light. The scintillator is always placed in contact with a photo-multiplier tube (PMT). When the visible light strikes the window of the PMT attached to a cathode, it will produce electrons. These electrons will be accelerated by the bias voltage to dinodes. In the process the electrons are multiplied and accelerated towards the anode at the end of a PMT, such that the signal now is amplified (Dove, 2003; Brown *et al.*, 1999).

In the next section, the feasibility study of Mineral-PET is reviewed and it is shown how the electronic signals are processed by a computer interface in order to produce an image which can be read by a human being.

2.2 Review of the feasibility of Mineral-PET

2.2.1 Introduction

It is highly desirable in diamond recovery operations to detect, at an early stage, the kimberlite materials which host the diamond inclusions and reject the barren kimberlite without loss of any diamonds. A careful approach to further processing of the kimberlite, with little danger of destroying the precious rock (diamond) would then be possible, since the position and the size of the diamond would be known when using Mineral-PET technology. The predetermination of diamond containing rocks would help to reduce the load, capacity, and time required of the downstream processing equipment.

As mentioned in Chapter 1, Mineral-PET is foreseen to be a very powerful tool for detecting and imaging diamonds for recovery on on-line mining and processing of kimberlite rock. The imaging and detection depends on the transmutation of a fraction of the carbon atoms in the diamond from carbon-12 to carbon-11. This transmuted isotope emits two back-to-back 511 keV photons, indicating the presence of carbon. To image the source of radiation, thereby identifying the full geometry and relative location of the diamond within the kimberlite material, quasi- (or full 3D-) imaging, is needed.

Mineral-PET is therefore based on two technologies originating from medical physics and hospitals:

1. The γ irradiation source and
2. the PET (positron emission tomography) imaging system.

The algorithm in Mineral-PET should be suitable for a conveyor belt type situation which is different from that of a hospital situation where there is little fluctuation movement, due

to inhalation by a patient. Therefore, the Mineral-PET has a fast sorting decision making algorithm based on statistical significance requirements. Energy and time responses are both essential in this practice.

The Mineral-PET computer receives the (x,y,z,t) coordinate pairs from the data acquisition system. Where x,y,z are events read from three dimensions x, y and z, and t is the time coordinate. These events are set and processed to draw tubes and counting voxels in the histograms, and the peak finder routine is called so that the higher events density can be determined.

2.2.2 Basic principles of mineral-PET physics

Positron Emission Tomography (PET) is a process in which a positron is used to image the positron source or the carrier of the source similar to Medical-PET where a carrier is an organ which is undergoing metabolism.

In Mineral-PET high energy γ photons are directed to a kimberlite rock which has carbon-12 as one of its constituents. The interaction of the photons with the carbon creates nuclear reactions. Among other reactions is the γ-neutron (γ,n) reaction occurring in the giant dipole energy region (GDR), which will result in the production of carbon-11. The following represents the gamma-neutron reaction in carbon-12:

$$^{12}\mathrm{C}(\gamma,\mathrm{n})^{11}\mathrm{C}$$

$$\downarrow$$

$$^{11}\mathrm{C} \rightarrow \beta^{+} + {}^{11}\mathrm{B}\ (\text{stable})$$

where the unstable carbon-11 emit positron, and then rearrange to stable boron-11. The positron emitted will, after it has thermalized, annihilate with an electron to give two γ

photons of 511 keV each as in the following expression:

$$e^- + e^+ \rightarrow 2\gamma \text{ photons}$$

From the carbon-11 β^+ emission, the positron emitted will lose its energy as it travels through the material (the positron is said to thermalize) and when its total energy is about 511 keV (energy equivalent to electron mass), it will combine with an electron and annihilate to two back-to-back γ photons each of 511 keV. These photons will then go into a matrix of detectors and deposit their energy as summarized in Figure 1.3. The energy deposited is proportional to the detected signal. One other important event is the time at which both the photons arrive at the oppositely placed detectors, from which it may easily be told if the photons are from the same annihilation process.

These two back-to-back photons are then detected through the photon interaction with the detector. The detectors in the system must be placed opposite to each other so that they can record the two photons released in opposite directions. When this kind of detection occurs the event is called coincidence. The localized high density γ photons as opposed to few spread low density from the kimberlite are assumed to be coming from concentrated carbon inclusion. In Mineral-PET this means the presence of a diamond in the kimberlite rock.

The high density is realized by the clustered interactions between the coincidences as they are detected by the detector arrays. This may include false interactions where photons from different annihilations may be detected simultaneously in the array. The rock itself has carbon as one of the elements, this may act as an interferer in the detected image. The carbon in the rock is almost homogeneously distributed and forms the background. All the background can be suppressed statistically.

Table 2.1: The chemical analysis of a few kimberlite samples (adapted from Ballestrero *et al.*, 2005).

	Weight (%)		
Component	Grey kimberlite	Altered Grey kimberlite	Black kimberlite
SiO_2	43.5	39.1	40.96
TiO_2	0.74	0.83	2.21
Al_2O_3	3.66	3.77	2.87
Na_2O_3	4.9	4.05	5.03
FeO	2.7	2.89	4.28
MnO	0.16	0.25	0.1
MgO	27.85	36	27.25
CaO	3.64	0.42	6.02
Na_2O	0.2	≤ 0.1	0.71
K_2O	0.67	0.2	1.22
H_2O+	8.2	9.89	7.47
H_2O-	0.91	1.89	1.1
P_2O_5	0.15	0.13	0.19
CO_2	0.2	0.22	0.15
Total	97.48	99.64	99.56
Ni [1]	1354	950	1338
Cr [1]	728	752	1370
Sr [1]	139	79	n.d.

In parts per million[1]

Other elements in the kimberlite may also interfere with the detected image. Oxygen, mostly present in oxides, is the main cause of interference. This oxygen forms 50% of the rock (Table 2.1) and is also a positron emitter, and therefore forms coincidence interactions. Due to its shorter lifetime ($\tau \sim 2$ min) compared to carbon ($\tau \sim$20 min) (Ajzenberg-Selove & Lauritsen, 1968; Behrens *et al.*, 1975), the imaging of diamond carbon-11 is possible. Other positron emitters include ^{13}N, ^{18}F, ^{45}Ti, and ^{64}Cu. The combined contribution of all the PET isotopes interferences amount to 20% of the background signal after a 20 min waiting period after irradiation and is expected to be homogeneous.

The difference between Mineral-PET and Medical-PET is a special algorithm, that does not require high resolution full 3D-imaging as in Medical-PET. A fast sorting decision is made

based on statistical significance requirements. With a few positrons the sorting decision can be made as this only requires a high throughput and low activity. This type of sorting is easy, due to the high contrast ratio between the diamond signal and the background.

The giant dipole resonance (GDR)

When a γ photon (electro-magnetic radiation) passes next to a nucleus of an atom it provides an oscillating electric field that exerts a force of attraction on charged protons in the nucleus. The photon interacts with the electric field of the nucleus and as a result the protons are attracted to one place away from the neutrons. After the photon has passed the atom the protons attempt to return back to the neutrons. In doing so they oscillate and hence the whole system oscillates. When the system stops oscillating it has accumulated excess energy. When the protons return to the original positions, they release the excess energy in the form of γ rays or a neutron (Hidgson *et al.*, 1997; Kawatsu & Shevin, 2003). In the case of carbon, the γ energy is approximately 22.5 MeV. This is called giant dipole resonance (GDR) (Vertes, 2001; Lochstet & Stephens, 1966; Fultz *et al.*, 1966).

The algorithm of Mineral-PET

The Mineral-PET algorithm is designed in such a way that it will be suitable for a conveyor belt type situation (i.e. the imaged rocks will be moving on a transport mechanism). This is typically the first step of the online processing of kimberlite rocks. The transported rocks will pass through an imaging device (array of detectors). A two dimensional shadow of the material along with the time component is constructed by the software algorithms to form a three dimensional (3D) representation of the material on the conveyor belt. The quasi-imaging Mineral-PET device, which works in an analogous way to the Medical-PET but with a faster algorithm, is used instead (Colsher, 1980). The Mineral-PET system has a higher contrast in the PET isotope distribution.

The two back-to-back photons lead to a "tube" along the emission line with a width equal to the position resolution (between 1 and 2 mm) of the detector. The non-PET events are filtered primarily by this coincidence condition, with the coincidence window of 2 ns. The random coincidence rate from activated non-PET isotopes is expected to be less than 1% as described in section 2.2.3. Therefore the secondary filter is the energy resolution with the energy acceptance window set to include a substantial portion of Compton events from 511 keV photons. The remaining background comes from non-diamond carbon and PET isotopes other than carbon. Oxygen-15 (^{15}O) as discussed in section 2.2.3 is the only significant remaining background and can be eliminated by developing a hold hopper (see Figure 1.1) which allows for a 20 min (10 half-lives) delay for it to decay out. The Mineral-PET algorithm looks for a statistically significant hot-spot of localized carbon, as the non-diamond carbon is assumed to be homogeneously spread in the entire kimberlite. This is termed the tube clustering detection method.

The quasi imaging is not a full 3D- imaging as in Medical-PET, but is sufficient to give some level of information on the source location of a PET isotope. The hit position of each end of the annihilation line or "tube" is recorded by the position sensitive γ detector, and the tube is recorded within their detection volume generated in a computer memory array. A 3D-histogram is incremented to generate a "tube density distribution". The motion of the conveyor belt is compensated by times stamping the γ coincident events. A typical conveyor belt would be 1 m wide and move at 2 m/s and this is corrected for in the algorithm.

The 3D-histogram gives a tube density distribution with a voxel size (approximated to 5 mm) given by the absolute resolution of the system. The resolution is determined by the range of the positron path before its annihilation (about 1 mm) (Levin, 1999), the position resolution of

the detector (about 2 mm), and the geometry of the detectors (which may make the tube voxel non-cubic and give a parallax effect). A 3D-histogram will contain events originating from (1) real intersections of the tube from PET isotopes in the diamond, (2) real intersections of the tubes from non-diamond carbon, and (3) false intersections of the tubes where the intersection is by chance and not correlated with a carbon source point.

All diamonds will lead to a real intersection at the position of the diamond incrementing the 3D-histogram if the diamond size is smaller than the voxel size. Some tubes are lost due to efficiency arguments. The following equation represents the number of real intersections from diamond:

$$N_{\cap} = \varepsilon^2 \frac{\Delta\Omega}{4\pi} \Delta t A(t) \tag{2.1}$$

Where Δt is the period of detection. A(t) is the activity after waiting period (20 min) in the hold hopper. $\frac{\Delta\Omega}{4\pi}$ is the solid angle of detection, and ε is the efficiency of each detector. The detector system of mineral-PET is a two-fold coincidence detection system because the photons are back-to-back, therefore one annihilation hits two detectors at the same time, hence the ε^2 term. If one detector captures a photon the other definitely will. The solid angle factor for the geometric efficiency occurs only once for both detectors, hence it is not squared.

The tubes from non-diamond PET isotopes can lead to an incrementation of the voxels in a 3D-histogram because of the statistical probability of the intersection with another tube somewhere in the detection volume not located at the true source point of both tubes (Hoffman, Huang & Phelps, 1981), referred to as false intersection.

Consider a sensitive cubic volume of $u \times u \times u = u^3$ voxels, where l is the actual length of the detection volume and r is the resolution of the detection system, then $u = l/r$ and the probability of any given voxel being incremented is $p = \frac{1}{u^3}$. If the number of tubes from

non-diamond isotopes is N, then Nu events must be distributed over the 3-D histogram in a homogeneous background. Consider that a tube will increment u voxels. The average number of tubes in a voxel which the real diamond coincidences (of size smaller than a voxel) will be measured against is B (background). Therefore, the number of background intersections per voxel is

$$B = Nup = \frac{N}{u^2} \tag{2.2}$$

If the number of tubes detected from a diamond is $N_\cap$, then the number of tubes detected from non-diamond carbon, N, are related by the formula

$$N = N_\cap \times R \tag{2.3}$$

where R is the ratio of mass of non-diamond carbon (represented here by sub-script NDC) to that of diamond (represented here by sub-script D). Therefore

$$R = \frac{m_{NDC}}{m_D}$$

Considering the minimum required size for a diamond to be detected is 1 mm^3 (0.5 ct), the mass of diamond $m_D = V_D \times \rho_D = 0.001$ $cm^3 \times$ 3.5 g/cm^3 = 0.0035 g, and the mass of non-diamond carbon is calculated as follows: $m_{NDC} = V_{NDC} \times \rho_{NDC}$ and the density of non-diamond carbon $\rho_{NDC} = P_{NDC} \times \rho_K$ where P_{NDC} is the atomic percentage of non-diamond carbon and ρ_k is the average density of kimberlite.

We know the weight percentage of CO_2 in kimberlite is 0.2%, which means P_{CO_2} is $\frac{2}{1000}$ (Table 2.1).

The molecular mass ratio of carbon to carbon dioxide is $\frac{M_C}{M_{CO_2}} = \frac{12}{44}$. This term extracts only the percentage of carbon in the CO_2.

It therefore implies that $P_{NDC} = \frac{M_C}{M_{CO_2}} \times P_{CO_2}$

$$= \frac{12}{44} \times \frac{2}{1000}$$

$$= 0.00055$$

Therefore $\rho_{NDC} = 0.00055 \times 2.8$ g/cm^3 $= 0.00153$ g/cm^3.

Considering a typical kimberlite rock with a linear size of 10 cm, at its largest value (i.e for the smallest diamond and therefore weakest signal) typically, and a tube resolution r to be 5 mm $m_{NDC} = 1000$ cm$^3\times$ 0.00153 g/cm^3 $= 1.53$ g

R equals to 437 and therefore N $= 437\ N_{\cap}$.

Substituting N in equation 2.2 and $u = l/r = \dfrac{10}{0.5} = 20$, the Background (B) $= 1.093\ N_{\cap}$

For each tube the filling of voxels may be regarded as a binomial distribution which can then be approximated by a Poison distribution. Therefore, the probability of n intersection events found in any particular voxel is (Ballestrero *et al.*, 2005)

$$P(n, N, p) = \binom{N}{n} p^n (1-p)^{N-n} = \frac{(B)^n e^{-B}}{n!}$$

So the error bars of the background of the tube distribution is Poison, and therefore

$$\sigma_n = \sqrt{\bar{n}} \simeq \sqrt{n}$$

The typical concentration of non-diamond carbon is taken to be less than 0.2% of the whole kimberlite (Table 2.1). A diamond (1 mm size) is taken to be the worst case in the detection, which means it is the smallest size that this algorithm may detect. If we calculate the number of intersections necessary to have the diamond signal appear above the background at 80% confidence level (CL) so that a diamond of 1 mm can be detected, we should first average background anticipated.

Consider 1.6 $\sigma_{N_\cap}$ or 80% confidence limit, then $\frac{N_\cap}{\sqrt{N_\cap + B}} > 1.6$. But B = 1.093 $N_\cap$. Therefore $\frac{N_\cap}{\sqrt{N_\cap + (1.093 N_\cap)}} > 1.6$. The total number of real intersections/tubes ($N_\cap$) which emerge as a 1 mm diamond signal is 5.4.

Consider now the acquisition time of 1 second with the solid angle $\Delta\Omega = 2\pi(1-cos\theta)$, $(\theta = 45^0)$ and the detector efficiency of 30%. The radiation activity A(t) of the diamond associated with these $N_\cap$ calculated from equation 2.1 is concluded to be 410 Bq. This activity is further used in the calculation of the electron flux in order to get the accelerator beam current in section 3.5.

2.2.3 Background and interferences

Non-diamond carbon in the kimberlite host material

Kimberlite are explosive breccia originating at a depth of about 150 km beneath the surface of the earth. Volcanic eruptions result in fragments of the mantle being transported to the earth's surface, including the diamond bearing rocks. Three types of Kimberlite (named after Kimberley, a town in the Northern Cape, Republic of South Africa) are known and have varied percentage weight of components as shown in Table 2.1. The physical composition also reflects the tumultuous nature of the formation of the breccia. Because of the violent nature of the extrusion processes, the non-diamond carbon will have a low density. Since diamond is durable, it is most likely that the concentrated or localized high density forms of carbon are in the form of diamond.

The tube clustering detection technique can only give evidence of the existence of the element carbon but cannot distinguish between different physical forms of the element. If we consider a typical size of a kimberlite rock as 1000 cm^3 (10 cm $\times$ 10 cm $\times$ 10 cm) and the volume of a typical diamond of 0.5 ct, we realize that the background radiation will be relatively large.

One then expects the diamondiferous kimberlite to have on average only 14% more carbon content than the barren one.

Therefore there is a need to introduce some extra measures so that the barren kimberlite can be distinguished from the diamondiferous kimberlite. The quasi-imaging system is used because it exploits the fact that diamond sources of carbon are expected to be more localized than non-diamond sources. Since the quasi-imaging algorithm looks for carbon hot-spots in the material, it may be viewed as lowering the contribution of the background carbon signal by discriminating a smaller logical volume of material than the actual physical volume of the kimberlite material. It thus becomes partially independent of the size of a typical kimberlite as mentioned above, though the feasibility calculation limits the size of diamond that can be detected to a minimum of a 1 mm.

Interferences from other activated elements in kimberlite

When kimberlite is activated for carbon detection, other elements which are composites of the rock are also activated. These elements may cause interference during the detection and contribute to large background γ rays. As indicated in Table 2.2, most of the radionuclides formed have a very short half-life compared to the most abundant element oxygen. Oxygen-15 is a big concern, since it contributes 50% in weight percentage to the kimberlite rock and may totally mask the carbon γ signal to the detector. This problem may be overcome by placing the irradiant kimberlite rocks in a hold hopper for 20 min. After 10 half-lives a radioactive element would have lost its activity by a factor of 1000, as indicated by the following calculation.

One half-life reduces the activity by a factor $(\frac{1}{2})^1$. Where $\frac{1}{2}$ indicates the mode of decay and the power 1 indicates the number of times that the radionuclide has undergone that mode. After 10 half-lives we have the activity factor of $(\frac{1}{2})^{10} = \frac{1}{1024}$. Therefore after 20 min the activity of ^{15}O would have decreased by more than a factor of 1000, whereas the ^{11}C would

decay only by a factor of two.

Table 2.2: Radionuclides resulting from photo-nuclear activation of the kimberlite rock as well as their half-lives (adapted from Ballestrero *et al.*, 2005).)

Elements		Radionuclide	and its	half-life		
Si:	^{24}Si-0.1s	^{25}Si-0.2s	^{26}Si-2.2s	^{27}Si-4.1s		
O:	^{13}O-8.9ms	^{14}O-71ms	^{15}O-2m			
Ti:	^{41}Ti-0.8ms	^{42}Ti-0.2s	^{43}Ti-0.5s	^{45}Ti-3.1h		
Al:	^{22}Al-70ms	^{23}Al-0.5s	^{25}Al-7.2s	^{26m}Al-6.3s	^{26}Al-7e5y	
Fe:	^{49}Fe-0.1s	^{51}Fe-0.3s	^{52m}Fe-46s	^{52}Fe-8.3h	^{53}Fe-8.5m	
Mn:	^{49}Mn-0.4s	^{10}Mn-1.7m	^{50m}Mn-0.3s	^{51}Mn-46m	^{52m}Mn-21m	^{52}Mn-5.6d
Mg:						
Ca:	^{36}Ca-0.1s	^{37}Ca-0.2s	^{38}Ca-0.4s	^{39}Ca-0.9s		
Na:	^{20}Na-0.4s	^{21}Na-22s	^{22}Na-2.6y			
K:	^{35}K-0.2s	^{36}K-0.3s	^{37}K-1.2s	^{38m}K-0.9s	^{38}K-7.6m	^{40}K-1e9y
H:						
P:	^{28}P-0.3s	^{29}P-4.1s	^{30}P-2.5m			
C:	^{9}C-0.1s	^{10}C-19s	^{11}C-20.3m			
Ni:	^{53}Ni-0.1s	^{55}Ni-0.2s	^{57}Ni-36h			
Cr:	^{45}Cr-0.1s	^{46}Cr-0.3s	^{47}Cr-0.5s	^{48}Cr-22h	^{49}Cr-42m	
Sr:	^{79}Sr-2.1m	^{80}Sr-1.8h	^{81}Sr-22m	^{83}Sr-1.4d		

2.2.4 Radiation protection issues in Mineral-PET

The protection of people and the environment against experiments or operations resulting in ionizing radiation must be taken into consideration. People can be exposed to radiation either by ingestion or external exposure. The measures to protect against ingestion and external exposure are similar to general occupational health and safety methods (i.e. use of protective clothes, enough ventilation, filtration, limiting exposure time, etc ...). Methods of shielding against radiation are unique to radiation control (Shapiro, 2002). In this section we consider the plant, the bulk kimberlite and the product of interest which is the diamond as potential radiation sources. Feasibility calculations concerning the emissions from these components are discussed.

The plant

It is important that the planning and construction of the plant is safe. The plant will be a localized radiation zone, and it is anticipated that long lived radionuclides will have a very long half-lives that their safety effect will be very low. However, there are short lived radionuclides which will produce very high radiation during the activation. A study by Chinaka, *et al.*, (2012) shows that a shield of about 1.6 m thickness is required. The shield consist of lead, iron, Wax, and boron carbide.

The kimberlite

After the process of detecting if the rock has diamond or not has been completed, the rock will still be radioactive. The remnant kimberlite activity is expected to be coming from the carbon content of the kimberlite, the carbon of the diamond, inclusions within the diamond, and other long lived isotopes in the kimberlite.

If a sample is irradiated with bremsstrahlung photons which have been generated from a 40 MeV electrons beam at a photon-dose of 10^{13} $cm^{-3}h^{-1}$ for E_γ >15 MeV and at an irradiation period of 1 h, the image in Figure 2.2 is obtained. The diamond signal is 400 times stronger per voxel than the kimberlite signal. The blue area shows the homogeneous distribution of background non-diamond radiation and the darker colour corresponds to a diamond radiation as it appears in a 3-D figure above. The centres of the diamonds are approximately 10 mm from each other. In this Figure it can be observed that the kimberlite activity is dominant by an order of 2 to that of carbon based activity at short times. The largest lifetime component is about 0.5 day in the short time activity.

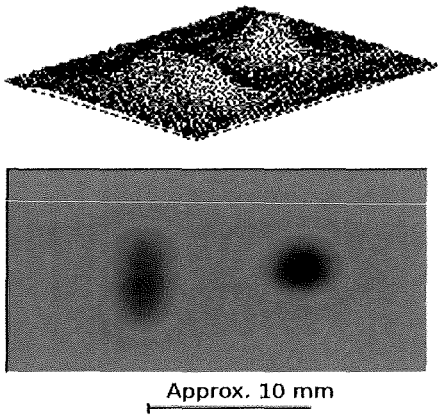

Figure 2.2: Diamond particles placed behind a kimberlite rock and then irradiated in a medical γ facility and subsequently observed in a Medical-PET facility.

The inclusion in diamond

To address the activity from inclusions within the diamond, a large sulfide inclusion was irradiated for 1 h. The activity decay of this substance showed an exponential decay which fit perfectly with the half-life of carbon-11. No other significant activity contributions were

indicated in the activity spectrum. After two hours the absence of any long lived components was confirmed by irradiating other inclusions-rich diamonds. Given the fact that inclusions in the test sample were large and that the remnant activity was created at higher irradiation doses than necessary for imaging, and no remnant non-511 keV activity could be defected (Ballestrero *et al.*, 2005), the remnant activity from inclusions in diamond is not seen to be a problem.

Considering the activity on the diamond, the half-life of a photo-nuclear transmuted carbon is 21 min (Table 2.2), and the fact that the boron daughter (^{11}B) from β^+ decay of ^{11}C is a stable element, it will not be possible to detect any remnant activity in the bulk of irradiated diamond after one day.

2.2.5 Radiation Damage

The interaction between photons and the carbon lattice is only through secondary processes such as the Compton effect to produce electrons, pair production to produce pairs of positrons and electrons (as explained in Chapter 1), and nuclear reactions. The secondary particles as well as the recoil from the reactions are extremely rare. The irradiation dose delivered by an intense beam is for a very short period, a fraction of a second. In tests during the feasibility study, it was found that several hours of irradiation are required to produce significant damage. Therefore the generation of vacancies and interstitials are at least several orders less than the threshold for visible damage in a diamond. This is confirmed in the calculation of the number of ^{11}B converted irradiation of 1 sec, which will be shown in section 3.5.

Remnant longer term issues

The remnant longer term activity contribution is almost zero because the remaining radionuclides have a very long decaying time. The half-lives are in orders of years, for example Al and K (Table 2.2). The activity $A = \frac{N}{\tau}$, where N is the number of decaying events and τ is the life time of the isotope is therefore low.

Conclusion

In conclusion, this review has shown how the physics in Medical-PET has played a role in bringing about the idea of Mineral-PET, and also the feasibility of the Mineral-PET.

Chapter 3

Methodology

3.1 Introduction

In this chapter it is discussed how the apparatus for testing the Mineral PET are prepared and tested. the apparatus include detectors, phantoms and the final counting station.

3.2 Detectors

The type of detector to be used in the mineral-PET was chosen after the efficiency of the detectors was investigated. Detector properties like time and position resolution played an important role in determining the efficiency, because not only the size but also the position of the detected diamond needs to be determined (Yamamoto, 1981).

The environment in which the detector has to be operated requires that a robust and less hygroscopic detector be used. BGO detectors are more suitable for this type of application, compared to other inorganic scintillator detectors, such as LSO and Na(Tl), which are widely used in medical PET because it is robust and not expensive (Blasse, 1994). The properties of

BGO are given in Table 1.1.

The BGO detectors are arranged in an array form and the arrays are placed opposite to each other in order for them to be able to detect annihilation. This set of detectors are then connected to electronic modules for signal recording, and further connected to a computer for signal processing. The whole set of modules (i.e. amplifiers, gate and delay, time to pulse height converter (TPHC), etc...) is called the data acquisition system (DAQ).

3.3 Phantoms

As in medical-PET the algorithm and the efficiency of the system was tested by means of detecting the activity on a phantom. To test for detector capabilities and efficiency in this project, phantoms with properties similar to the real samples were constructed.

A positron source which resembles the activated carbon in a kimberlite as closely as possible was used to resemble a diamond inclusion and a homogeneously spread non-diamond carbon in a kimberlite. The composite of the phantom kimberlite should also be as close as possible to the real kimberlite. The active phantom should resemble a PET active kimberlite after the 20 min hold-hopper delay time.

Sodium-22 as a positron emitting radio-isotope was used as both a hot-spot that resembles diamond and the possible background inclusions. It was chosen because it has a half-life ($\sim$ 2.6 years) long enough to make the efficiency tests. Re-calibrated measurements of existing ^{22}Na were done to measure how much of the radionuclide would be used to make the desired size of the dummy diamond and background.

Method of phantoms preparation

The kimberlite rocks were crushed to a very fine powder and mixed to form a homogeneous mixture of all elemental compositions. The crush lab available at iThemba (Gauteng) was used to produce the powder. The powder was reconstructed with a binder and in the process ^{22}Na (available as NaCl) of a specified volume was added at a position relative to the centre of the reconstructed rock. Polyvinyl alcohol was used as the solvent because it is volatile and it dries very quickly reducing the possibility of the radionuclide migrating from the planted position. Polypropylene was used as the holder for the ^{22}Na, to insure that it stays in place.

Building cement was used as a binder to keep the powder together and to close the air voids within the phantom. The phantom container was shaken with a vibrator to allow the mixture to settle, not too vigorously as that could introduce more airspaces and change the position of the hot spots. A polymer plastic was used as a container to ensure that if an accident occurred the phantom would not break and cause a radiation hazard.

A press machine was used to keep the phantoms packed and hence improve the density and keep it close to that of a real kimberlite.

The positions were marked for position identification when testing the detectors. Five sizes (volumes) of ^{22}Na and a combination of two sizes at different positions relative to the centre of a phantom were considered. Fourteen constructed phantoms with ^{22}Na and one with no hot spot (used as a control for background readings) were constructed.

The ^{22}Na was inserted in the phantom as follows: The kimberlite powder was mixed with a certain amount of polyvinyl alcohol and a binder (15% cement + wood-glue). Half of the phantom shape was molded. The ^{22}Na was then placed at a relevant position, then the other

half placed on top to complete the whole volume. The phantom was then allowed to dry for ten minutes.

^{22}Na was placed in polypropylene which served as a primary container of ^{22}Na before it was placed in the phantom.

Activity measurements

The activity of a phantom should be the same as that of the anticipated activity and therefore was calculated using equation 3.1.

3.4 Specification of a typical final counting station

The total number of detectors in an array of 4 m^2 is 80, each at 50 cm^2. Such a system is specified to process a load of about 1000 tons per hour. The data acquisition system (DAQ) is a system of 80 $\times$ 4 channels. The number 80 specifies the number of detectors and 4 the number of signals from each detector. The accelerator for γ production is expected to consume 1 MWatt of power. The counting station is estimated to cost \$11M which includes position sensitive detectors, the data acquisition and processing system, accelerator, radiation protection, and mechanical and civil engineering.

In the next section, activation calculations are done in order to get the actual accelerator current.

3.5 Calculation of Activation

The activation of kimberlite rock is the first of the essential steps in Mineral-PET. In this step a beam of electrons impinges on a target of high atomic number and produces bremsstrahlung with varying high energies. The bremsstrahlung then induce a photo-nuclear (γ, n)- reaction at the giant dipole resonance of an element of interest (^{12}C) and as a result it is converted to a detectable radioactive element (^{11}C). In this chapter, the processes involved in the activation are considered and electron flux is calculated with the aim of optimizing the accelerator beam current.

3.6 Photo-nuclear activation of PET isotopes

The photo-nuclear activation technique is also used in Medical-PET to produce radio nuclides. Although this method has not found widespread use in nuclear medicine because of the low radioactivity yield (Sorenson, Cheryl & Phelps, 1987), it could be very much appreciated in Mineral-PET, since the low radioactivity yield eases concerns on environmental radiation protection issues and yet is still able to produce desirable results.

In mineral-PET this technique produces high energy bremsstrahlung in the energy range of 20 to 30 MeV which correspond to the energies of the giant dipole resonance (GDR) of ^{12}C at which the (γ,n) nuclear reaction will occur. The GDR cross-section has been shown to be the highest at approximately 22 MeV (Fultz *et al.*, 1966; IAEA, 2000; Cook *et al.*, 1966; Barber *et al.*, 1955; Wolf & Redvanly, 1977).

In order to reach the GDR energies of the bremsstrahlung, the energies of the incident electron beam must be set higher than the GDR. Simulation (refer to Chapter 4) was done and the

energy was optimized to 40 MeV. The spectral energy distribution of the bremsstrahlung follows the Beth-Heitler theory, which is essentially $1/E_\gamma$ behaviour. This implies that to get enough photons of the desired energy, more electrons than the expected photons needs to be irradiated. In the spectrum, the high energy photons are less prolific. Figure 1.2 illustrates the energy spectrum of the photons and the resonance region of the photo-nuclear reaction that produces carbon PET isotopes.

Considering an average 10 cm^3 coarse crushed kimberlite of 2.8 g/cm^3 density, the irradiation depth should be at least 40 cm in order to use photon irradiation with 95% efficiency. This was confirmed with the use of a 13 cm material with attenuation of 50% of 30 MeV photons. For each photon produced there are typically 100 incident electrons bombarded on a metal target.

After the kimberlite is activated for the detection of diamond it will remain radioactive. That may cause a concern about the quality of the diamond as the product of interest and also kimberlite as it should be disposed back to the environment. Section 3.7 addresses this concern.

3.7 The activation process

During the activation process the transmutation of carbon, as it occurs through the GDR, will have an activity related to the irradiation parameters as follows:

$$A(t) = \{t_\gamma N_{^{12}C}(e^{-x/X_o})(\phi_{e^-}\frac{1}{\Delta E}\int_{\Delta_E} P_{e^-\rightarrow\gamma}(E)\sigma_{(\gamma,n)}(E)dE)\}\lambda_{^{11}C}e^{-\lambda_{^{11}C}t_h} \qquad (3.1)$$

The equation was derived as follows: The cross-section of the GDR is given by $\sigma_{(\gamma,n)} = \frac{R_n}{I_a N}$ where R is the rate of outgoing neutrons, I_a is the current of incident particles per unit time, and N is the number of target nuclei (Krane, 1988). Therefore

$$R_n = I_a N \sigma_{(\gamma,n)} \tag{3.2}$$

If we now consider incident particles with continuous and varying energies, as is the case in mineral-PET, then equation 3.2 becomes an integral. Therefore

$$R_n = N \int_{\Delta_E} I_a(E)\sigma_{(\gamma,n)}(E)dE \tag{3.3}$$

where $I_a(E) = \phi_{e^-} P_{e^- \rightarrow \gamma}(E)$

ϕ_{e^-} is the flux of incident electrons and $P_{e^- \rightarrow \gamma}$ is the probability of the electrons to convert to γ photons. Equation 3.3 can now be written as

$$R_n = N\phi_{e^-} \int_{\Delta_E} P_{e^- \rightarrow \gamma}(E)\sigma_{(\gamma,n)}(E)dE$$

The activity of the activated kimberlite measured after some time t_h (time delayed in the hold hopper) is expressed as

$$A(t_h) = \lambda_{^{11}C} N_{^{11}C} = \lambda_{^{11}C}(R_n \Delta t e^{-\lambda_{^{11}C} t_h})$$

Considering that this activity is measured out of the annihilation activity and that the annihilation traverses the kimberlite before it can be detected, the term e^{-x/X_o} is also introduced into the equation above. This term considers the attenuation of photons in the kimberlite, where x is the length at which the photons will propagate, and X_o is the radiation length.

Therefore the activity is expressed as :

$$A(t_h) = \lambda_{^{11}C} N_{^{11}C} = \lambda_{^{11}C} \Delta t e^{-x/X_o} N \phi_{e^-} \{\frac{1}{\Delta E} \int_{\Delta_E} P_{e^- \rightarrow \gamma}(E)\sigma_{(\gamma,n)}(E)dE\} e^{-\lambda_{^{11}C} t_h}$$

where t is time of the irradiation, $N = N_{^{12}C}$ and it is the number of carbon nuclei in the diamond which are illuminated by the beam of γ photons.

Two important factors must be considered. Firstly, whether there is sufficient electron flux (ϕ_{e^-}) to produce the required activity, which will be calculated later using equation 3.1. Secondly, when the product is activated, is it still worthy to be used as a recovered diamond. The latter question is answered in the next section by determining the amount of ^{11}C expected to be produced in a diamond during activation.

The amount of ^{11}C in Mineral-PET activated diamond

Let us consider the following calculations:

The number of ^{11}C produced in a single irradiation will be given by:

$$N_{^{11}C} = r.t_\gamma$$

where r is the rate of ^{11}C production and is given by $f.n_t.\sigma_\gamma$, and t_γ is the irradiation period.

therefore $N_{^{11}C} = f.n_t.\sigma_\gamma.t_\gamma$

where f is the flux of γ photons, n_t is the number-thickness of the material, and σ_γ is the γ cross-section of the material.

If we consider the following data f= 10^{14} γ/sec , σ = 8 mb = 8×10^{-27} cm^{-2}, t_γ = 1 s

and that the number thickness (n_t) is given by $\frac{\rho}{M_r}N_A t$

where t denotes the thickness of the material, other symbols retain their usual meaning, then a typical kimberlite rock of 10 cm thickness will give $N_{^{11}C}$ equal to 6.742×10^{12} of ^{11}C nuclei. The ratio of converted ^{12}C to those of existing ^{12}C is 1.12×10^{-13}. Where M_r for Carbon is 12 and ρ is 3.5 g/cm^3.

This number is very small and it means there should be no concern about the quality of the diamond product, since the change will be insignificant and will be difficult to notice even with the most sensitive devices.

The electron flux

Determining if sufficient electron flux (ϕ_{e^-}) can be produced, equation 3.1 is used. The activity of a 1 mm diamond calculated from equation 2.1 is 410 Bq, therefore substituting the activity in equation 3.1, the minimum electron flux required in Mineral-PET can be obtained.

$$\phi_{e^-} = \frac{A(t)}{\{t_\gamma N_{^{12}C}(e^{-x/X_o})\frac{1}{\Delta E}\int_{\Delta_E} P_{e^-\rightarrow\gamma}(E)\sigma_{(\gamma,n)}(E)dE)\}\lambda_{^{11}C}e^{-\lambda_{^{11}C}t_h}}$$

When the following values were substituted in the equation:

$A(t) = 410$ Bq.

$t_\gamma = 1$ s, $t_h = 20$ min,

$N_{^{12}C} = 1.76 \times 10^{20}$ atoms,

$e^{-x/X_o} = 0.33$, where $X_o = 9$ cm and assuming a 10 cm thickness of kimberlite and with the diamond at the centre.

the integral $\frac{1}{\Delta E}\int_{\Delta_E} P_{e^-\rightarrow\gamma}(E)\sigma_{(\gamma,n)}(E)dE$ is the product of the bremsstrahlung production probability or cross-section of photo-nuclear reaction which equals to $8.00\times\ 10^{-27}$ cm^{-2}, and the probability of electrons at energy range 22 - 27 MeV producing the bremsstrahlung photons. the probability of electrons producing bremsstrahlung is found by taking value of photon/electron ratio at FWHM on Figure 1.2 which is 1×10^{-4}. Therefore the integral equals to $8.00\times\ 10^{-31}$ cm^{-2},

$\lambda_{^{11}C}e^{-\lambda_{^{11}C}t_h} = 2.87\times10^{-4}$ s^{-1} for ^{11}C decay constant $\lambda_{^{11}C} = 0.0341$ min^{-1}. Therefore the electron flux is $3.04\ \times10^{16}$ cm^{-2}s^{-1}.

The accelerator current (I) is calculated as follows:

$$I = (N_{e^-}/t)q_{e^-} = A_b\phi_{e^-}q_{e^-}$$
$$= 3.04 \times 10^{16} * 1.60 \times 10^{-19} = 4.90 \times 10^{-3}\ Cs^{-1}\ (5\ \text{mA}).$$

where N_{e^-} is the number of particles (electrons) and A_b is the planar surface area of the perpendicular particle beam and is considered to be 1 cm^2.

Conclusion

It is indicated by the empirical model, experiments, and the Monte Carlo simulations that in order to process rocks at a typical mining rate of 1000 kg/s, the electron accelerator would have to be a machine with a continuous beam of 5 mA. A machine with this specification and modern technology would cost approximately $2M. This formed the basis of our investigation, and in Chapter 4, the kind of accelerator which will be used in the Mineral-PET is simulated.

Chapter 4

Simulation of photon production

4.1 Introduction

Simulation is done to create an ideal situation so that it will be easy to solve the real problems of the same or similar situations in investigations. The real life situation can then be manipulated to be brought closer to the ideal one. In this chapter the following two situations will be looked at: 1. The production of bremsstrahlung photons using accelerated electrons on the high atomic number metal; 2. The activation of the kimberlite rock by the produced bremsstrahlung. The efficiency of bremsstrahlung production at the electron moderator/converter material and after photo-neutron reaction on kimberlite will be specifically looked at.

The simulation is done using a code called Geant4, developed from C++ programming language. The Geant4 code was developed by a world-wide collaboration of physicists and software engineers participating in more than 10 experiments in Europe, Russia, Japan, Canada and the United States (Ferguson, 2000). It is editable by any user or developer, and is conveniently freely available. The simulation applies the Monte Carlo method for tracking particles

through matter.

To simulate the activation process, the apparatus which is needed includes: the accelerator for electrons; the moderator/converter for bremsstrahlung production; the detector; and the photons targeting the target/kimberlite. As explained in section 3.5 there should be a transmutation of ^{12}C to ^{11}C, therefore in this regard the concern is mainly about the bremsstrahlung at the cross-section of the ^{12}C photo-nuclear reaction. The moderator material, the electron flux and energy should also be simulated (Auslender *et al.*, 1999).

4.2 Geant4 code

Geant4 is an object-oriented toolkit developed to simulate the passage of a particle through matter. It is widely used in space physics, high energy physics, medical, nuclear and accelerator physics, and astronomy. It provides a complete set for all areas of detector simulation, including geometry, tracking, detector response, run, event and track management (Agostinelli *et al.*, 2003; Grichine *et al.*, 2000; Geani *et al.*, 1998).

It uses a random number generator among other utilities, which includes physics units and constants, particle management, interface to event generators and object persisting solutions. Software engineering techniques and object oriented technologies are used to validate physics results (Ferguson, 2000).

Geant4 consists of sub-codes as contributions from different developers and, as already mentioned above, the Geant4 source code can be edited by other users or developers. These sub-codes were merged into the mineral-PET simulation code (called converter) and modified to suit the mineral-PET problem (bremsstrahlung production). Geant4 can be used to define,

among other things, the target materials, the interaction processes, the incident particles, and tracking a particle through matter (Arce *et al.*, 1999).

Figure 4.1 shows the visualization in the simulation of NaI detector calibration measurements where ^{60}Co was used as the point source in the setup. The green lines show emission lines together with photons from material-photon interactions and the red lines shows electrons from the photo-electric interaction. The red insert on the detector part shows the NaI crystal, the gray shows teflon as a rapper for backscattering, and the pink is the borosilicate glass material as a window for PMT.

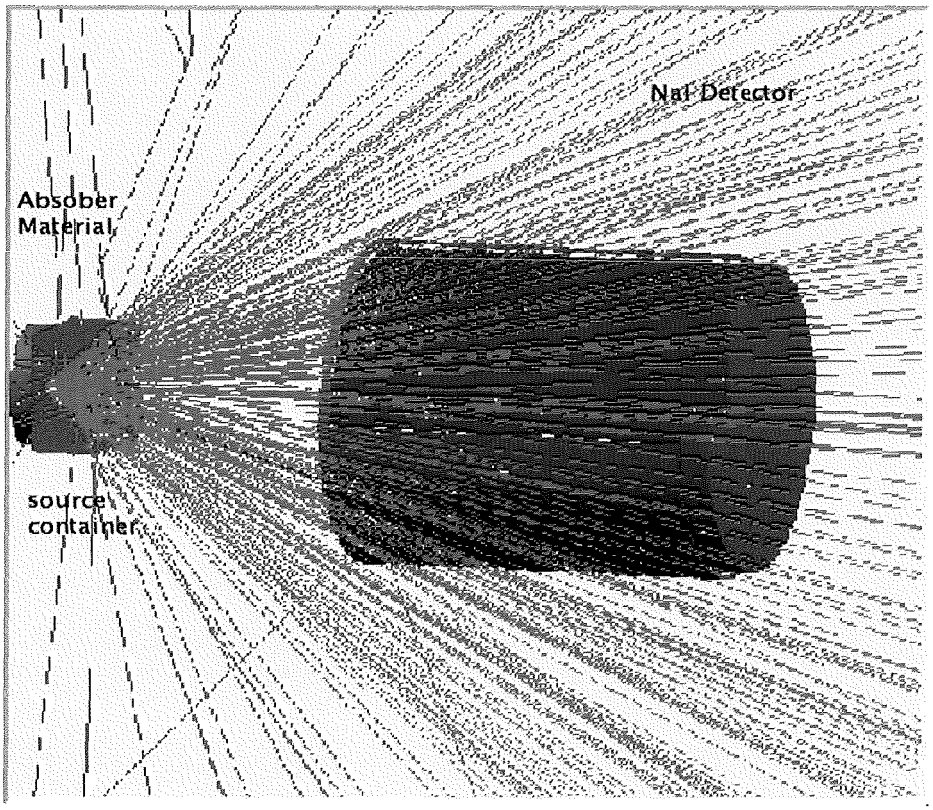

Figure 4.1: Experimental set-up for ^{60}Co absorption measurements using NaI detectors.

Computing requirements

A computer system of 2 GHz processor and Hard drive of 120 GB was adequate for the simulation of mineral-PET. Two million events were run for approximately an hour. The Geant4 code has an option of running in a visual mode which requires bigger memory space and faster computer processing speed. The advantage of the visual mode is that it can be verified that the code is performing as required and if the apparatus are placed at the correct places (see Figure 4.1). The other option is to run with no visual mode, which runs in the background and it is faster.

4.2.1 Monte Carlo methods

Monte Carlo methods are a numerical estimate of the solution by averaging over a very large number of iterated calculations. Hence they use fast memory access and the speed of modern digital computers. These calculations rely on the sequence of random variables used to sample from a distribution applicable to the problem. The real problem may be substituted with a stochastic one having the same solution (Ferbel, 1987).

Problems ranging from transport problems, statistical mechanics, mathematical problems, etc., may be investigated using Monte Carlo methods.

In Mineral-PET random electrons are produced and bombarded on a metal which will produce random bremsstrahlung. Calculations are done for different energies of electrons and even different thickness of materials. The results of our Monte Carlo simulation give the energy and the angle at which the photon has branched from the electron, which we plotted using an analysis programme called ROOT.

(Hammersley & Handscomb, 1964) give examples of radiation shielding, which is similar to

the production of bremsstrahlung in mineral-PET.

4.3 Validation of the simulation code

The validation of the Geant4 code was first made by measuring the radiation length of materials and then confirmed by measurements from a multi-channel analyzer system called DART/MCA-32. This process provided a reference for further analysis of properties of kimberlite rock and allowed results to be stated with confidence that these properties are a true reflection of the real situation.

The radiation length of aluminium metal was first calculated from absorption measurements done on the MCA-32 and then confirmed with the literature. Finally, the two values and the simulation results were compared.

The simulation has the capability of calculating the radiation length if it is fed with the correct atomic number and correct symbols for the element or component. This value was also obtained from the simulation before the calculation was made from the absorption measurements.

4.4 Simulation for accelerator

A setup in this simulation is shown in Figure 4.2 where the irradiation is done through two layers of kimberlite rock. The simulation considers irradiation from top to bottom of the hold hopper therefore irradiating through several layers of 10 cm thick kimberlite.

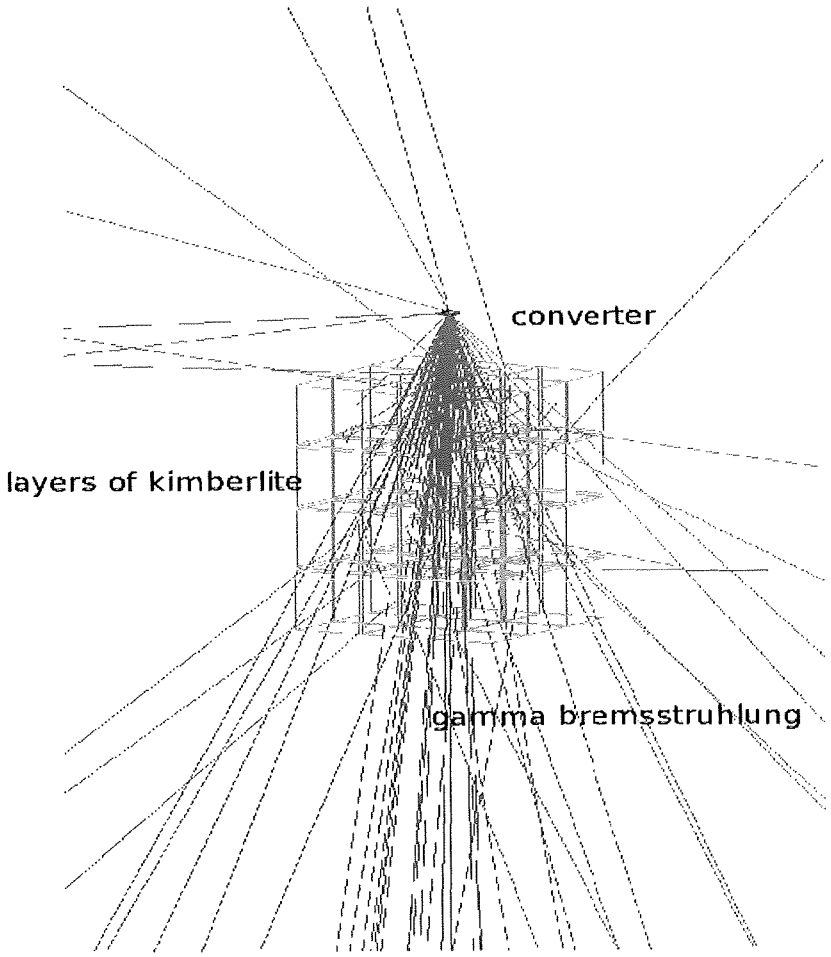

Figure 4.2: The simulation visualization of the irradiation process

Chapter 5

Results and interpretation

5.1 Results from the simulation of bremsstrahlung photon production

In the results two simulations are shown, the Mineral-PET and the Medical-PET. Figure 5.1 shows the representation of counts of γ photons against the γ energy, where the black graph is the simulation of the activation by the accelerator used for Mineral-PET and the red colour graph is the simulation of the activation by the accelerator used for clinical PET in Karolinska.

In the Figure it can be seen that at high energies, photons for the graph in black colour (Mineral-PET) dominate those of the graph in red colour (Karolinska medical facility). This is because of the difference in the thickness of the converters. The converter in the red graph is three times thicker than that in the black graph and it attenuates electrons with more power. The Karolinska accelerator is used for medical purposes and hence the thicker converter is used to block electrons as explained in section 6.2.

Figure 5.2 shows the propagation of γ bremsstrahlung through the converter to the target. 108 data points are plotted all at once after the simulation demonstrating the capabilities of

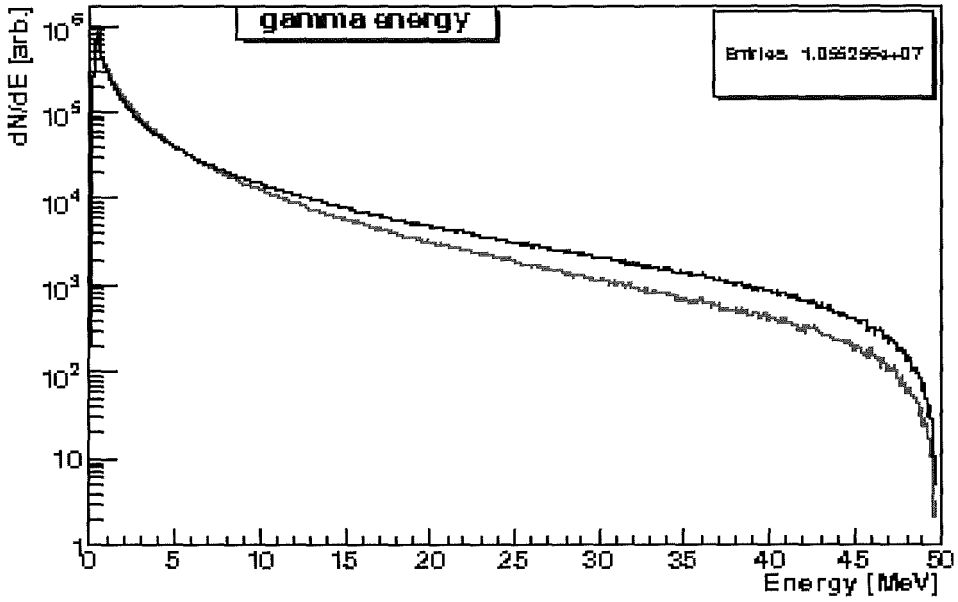

Figure 5.1: The production of bremsstrahlung as a function of energy where the red graph is for simulation of Mineral PET accelerator set up, while the black graph shows simulation of the setup at the Karolinska experiment.

Geant4 computing power. This Figure shows the production of γ photons per electron energy ranging from 20 MeV to 120 MeV and going through the different converter thicknesses. At this stage it was confirmed that the production of γ photons at continues even through the kimberlite of 10 cm thickness. Therefore, there are still more of the desired photons from the first layer which can be used on other samples underneath. This is due to the further conversion in the kimberlite by the high energy electrons that went through the converter to the kimberlite by scattering in a straight line or without scattering at all, as in Figure 4.2. Figure 5.3 shows that even after the irradiation of the second layer of kimberlite of the same thickness there are still more γ photons. Materials, W, Au and Cu were chosen on the basis that they have high melting points and high atomic numbers (see Table 5.1).

In all the plots, Figure 5.2, 5.3 (a), and 5.3 (b), gold and tungsten gave a good efficiency at the thicknesses equal to one radiation length. Copper is less efficient, at about 20% of the

Table 5.1: A table of radiation lengths for materials which were used in the simulation as adopted from the Atomic and Nuclear Properties of Materials for 292 substances (Groom, 2004).

Material identity	Atomic number(Z)	Radiation length/mm	Melting point(^{0}C)
W	74	3.5	3410
Pt	78	3.1	1772
Fe	26	3.3	1535
Cu	29	14.4	1083
Au	79	3.3	1064.43
Al	13	8.9	660.37
Cd	48	10.4	320.9
Pb	82	5.6	254

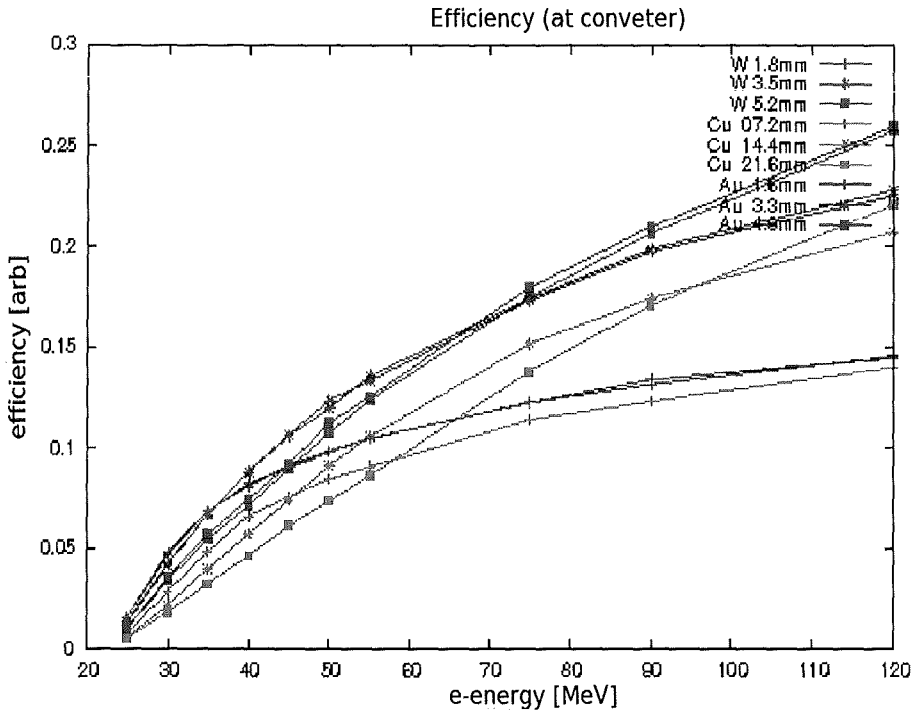

Figure 5.2: The efficiency of bremsstrahlung production as a function of energy, type ,and thickness of moderator at the converter level.

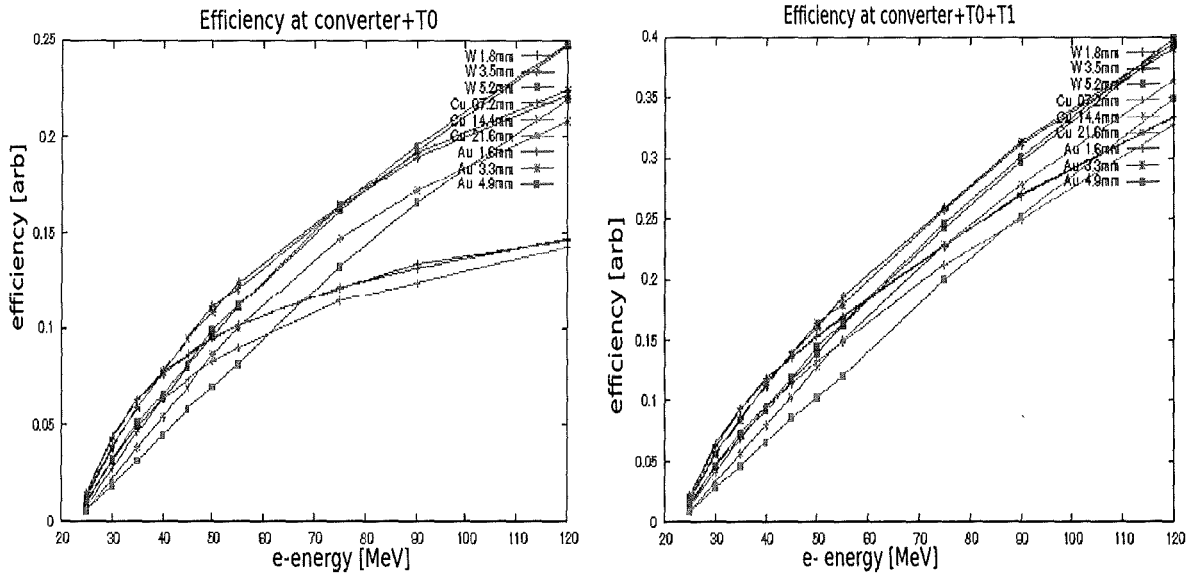

(a) (b)

Figure 5.3: 5.3 (a) Efficiency vs energy after the irradiation of single kimberlite layer, 5.3 (b) efficiency at second target layer.

efficiency of gold and tungsten.

The power efficiency is very significant in determining what electron energy should be used. The efficiency is then obtained by plotting electron energy against power $\left(\text{given by } \frac{(Ng/Ne)}{E/40}\right)$, where the 40 depicts that the results were normalized to the relative beam power, taken as E_e = 40 MeV as shown in Figure 5.4, and Ng and Ne are the number of γ's and number of electrons respectively.

Gold and tungsten have almost the same efficiency, but since tungsten is cheaper than gold, the optimum thickness of tungsten for γ photon production was investigated. The optimum thickness is obtained by plotting power efficiency against thickness, and the optimum thickness was determined as in Figure 5.5.

The grey line is a fitting curve and it shows the optimum thickness at 2.8 mm with 9% power efficiency. Dovbnya, Nikiforof & Uvarov, (2005) and Bocheck *et al.*, (1998) show the thickness

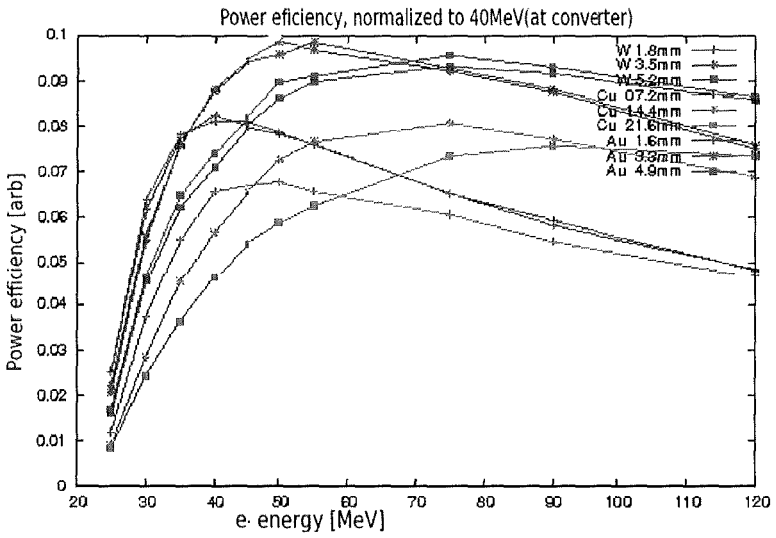

Figure 5.4: The power efficiency of γ production for W, Cu, and Au.

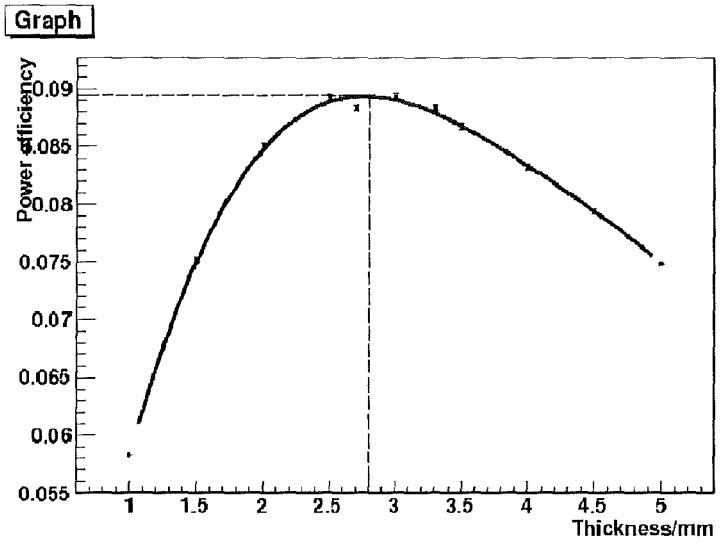

Figure 5.5: The optimum thickness of the converter material at energy 40 MeV.

of 3 mm at the same energy to be efficient.

To calculate the power loss on the converter to see if there will be a need to cool the system and by how much, and to achieve the maximum conversion factor of electrons energy to that of γ-radiation (Bocheck *et al.*, 1998), a plot of energy loss against electron energy was made in Figure 5.6.

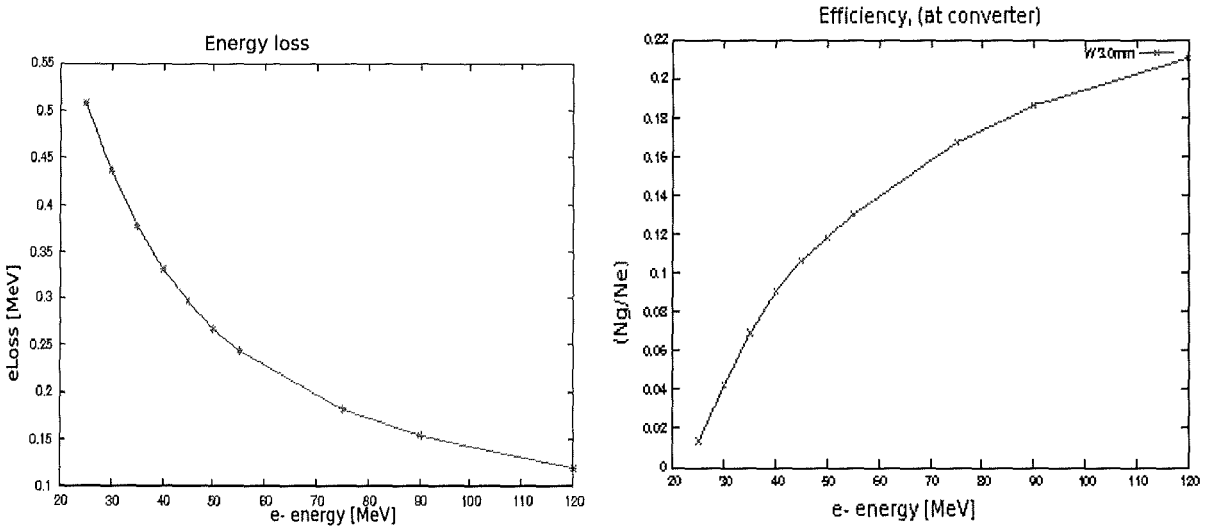

(a) (b)

Figure 5.6: (a) The energy loss at the converter (b) the efficiency of γ production at specifi 3 mm thickness.

If a specific point is chosen, say 40 MeV, it can be seen that the energy loss is 32.5%, or 13 MeV. The loss of energy is calculated by outgoing energy over the incoming energy. From this it can be seen that 27 MeV should be used in the converter.

Looking at the efficiency graph in Figure 5.6 (b) at 40 MeV, it can be seen that only 9% of the γ photons produced are the desired ones. The 27 MeV is used for this purpose, whereas the other remaining energy of the 40 MeV is used in producing low energy photons, a small fraction of photons of energies higher than 27 MeV photons, and the heat during collision. This proves that not much energy is lost in heat and therefore there is no need for intense cooling.

5.2 Angular distribution

Unlike the clinical PET where a narrow beam for tumour irradiation is desired, in Mineral-PET there should be a wide spread of the beam on the irradiants so that enough rocks can be covered. Therefore the angle of γ distribution was investigated.

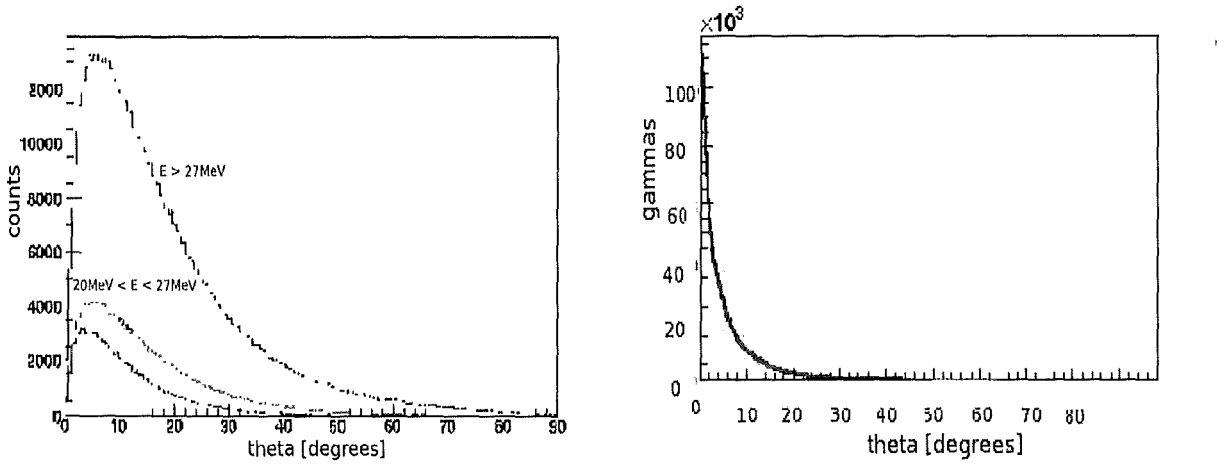

(a) (b)

Figure 5.7: 5.7 (a) The angular distribution at different energy range where the red curve indicates angles of γ's of energy between 20 and 27 MeV, 5.7 (b) Distribution of γ photons ranging from 20 to 27 MeV energy over angles between 0 and 90^o

Figure 5.7 (a) indicates the density of the beam (counts) against the distributing angle (theta). The curve in red provides for the energies ranging from 20 MeV to 27 MeV and it covers the range larger than 60^o. Figure 5.7 (b) shows the density of the photons of energies up to between 20 MeV and 27 MeV distributed over 0 to 90^o angles. It shows that the intensity of the photons at the region of interest covers a wider significant angle of 0 to 30^0.

The beam seems to spread to over 90^o, but as the angle moves away from 0^o the intensity of photons becomes weaker. The region of interest is for energies between 20 MeV and 27 MeV. It can be seen that this region is significant at angels from 0^o to 30^o. Because it is important that the photon beam covers the whole kimberlite during irradiation, and considering that the

irradiation area is within 1 m^3, it is found that the minimum distance between the irradiants and the photon source is approximately 1 m.

Chapter 6

Karolinska experiment

6.1 Introduction

To compare the simulation to real life situations an experiment was performed. Because Mineral-PET is a new project and did not have a facility, the experiment was conducted in a medical facility where there is a similar setup. At this particular time a demonstrator plant was under construction at iThemba LABS (Gauteng).

6.2 Overview of the experiment

The experiment was conducted in Karolinska-Sweden on a clinical LINAC (Linear Accelerator). The experiment had a slightly different set up from that of Mineral-PET because the converter thickness was three times thicker than that of mineral-PET. The reason for the difference in thickness is that this facility is for clinical irradiation, and therefore electrons must be absorbed before they get into the patient as they pose a danger to the patient's body tissues. If the electrons are not stopped, then they will stop in the patient's tissue and deposit all their energy because they do not have a longer range than that of photons, electrons' linear

energy transfer (LET) is larger than that of photons. They will, hence, do more harm than good. The other difference was that the beam of the Karolinska facility is more focused than the Medical-PET beam, which is expected to be spread over a wide area of irradiation. If the beam of the medical facility is not focused, then it will irradiate healthy tissues during the medical operation.

The time of irradiation was 180 seconds instead of the anticipated 1 second of Mineral-PET in accord with the feasibility study. This is because the thick converter was producing smaller γ/s for the activation than desired. Unlike the mineral PET beam which will be spread over a large area (1 m^2), the Karolinska medical facility has a focused beam with low photon flux, and therefore its beam current or power will be lower.

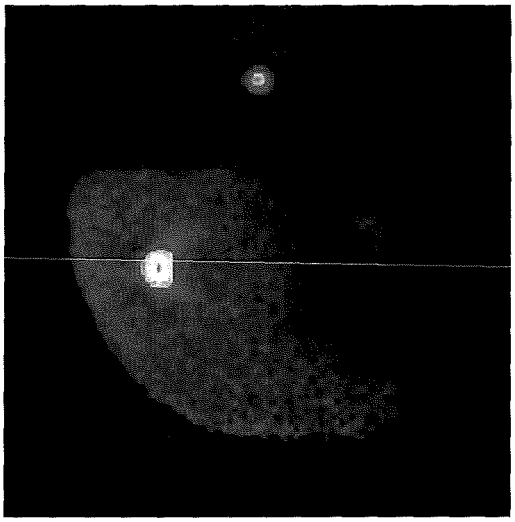

Figure 6.1: The reconstructed image of diamond in a kimberlite rock determined in Karolinska.

Figure 6.1 is the picture of the Karolinska test where a diamond was detected over a 1000 cm^3 kimberlite rock. The purple colour indicates the background colour from the test rock while the brighter intense colours indicate the diamonds. Less than 1 mm diamond is detected and is shown on the upper part of the picture.

In Figure 6.2 a series of images of the density distribution of PET isotopes, taken at three consecutive 20 minute intervals starting at within 10 minutes after the irradiation, are shown.

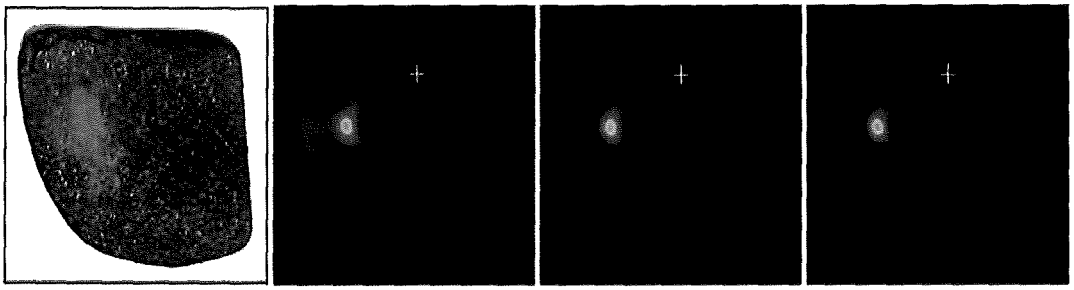

Figure 6.2: The reduction of background on diamond detection in kimberlite rock determined at Karolinska.

It can be noticed that the homogeneous background decreases with respect to the diamond signal at delayed time. The larger diamond is 0.5 ct and the larger kimberlite sample about 5 cm across.

Considering that the mineral-PET has a stronger beam intensity, it can be seen that these images would be improved. There would be more PET photons and therefore a faster and sharper image would be obtained.

Chapter 7

Conclusion

As the power efficiency of the accelerator at different material thicknesses is compared it can be observed that copper, tungsten, gold, iron and lead are the most efficient converter materials. However, other properties of these materials are a concern. Copper and lead are soft metals, therefore, if they are exposed to high energy radiation, then they can melt down. Gold is an expensive metal compared to the other four metals mentioned above. Tungsten of 3 mm thickness is as an ideal converter material considering its hardness, high melting point and the fact that it is relatively cheap compared to gold and other high Z materials.

Irradiating in a hold hopper shows to be more effective than in the conveyor belt where there is a single layer of kimberlite material. The efficiency improves with the addition of more kimberlite layers as the unreacted electrons on the first layer are collected and converted to bremsstrahlung photons to irradiate the next layer. Geant4 events tracking has been a powerful tool to prove that irradiation in a hold hopper is more efficient than irradiation on a conveyor belt.

The Karolinska experiment has proved the feasibility of mineral-PET by presenting results that show a diamond in kimberlite. These positive results will be improved with an up scale Mine Test Unit (MTU) at a suitable site in a real mining environment. Up to so far a small

scale technology demonstrator has been built at iThemba LABS where electronics, including detector system, had been tested.

It was shown that 40 Mev LINAC accelerator of 5 mA beam current is required to produce a minimum electron flux which can be used to activate the smallest detectable diamond. Though the Monte Carlo simulation in the feasibility study showed that a 50 MeV accelerator is 20% more efficient than a 40 MeV (see Figure 5.4), the latter is desirable because it is more cost efficient and cheaper to maintain.

References

Agostinelli, S., Allison, J., Amako, K., Apostolakis, J., Araujo, H., Arce, P., Asai, M., Axen, D., Banerjee, S., Barrand, G., Behner, F., Bellagamba, L., Boudreau, J., Broglia, L., Brunengo, A., Burkhardt, H., Chauvie, S., Chuma, J., Chytracek, R., Cooperman, G., Cosmo, G., Degtyarenko, P., Dell'acqua, A., Depaola, G., Dietrich, D., Enami, R., Feliciello, A., Ferguson, C., Fesefeldt, H., Folger, G., Foppiano, F., Forti, A., Garelli, S., Giani, S., Giannitrapani, R., Gibin, D., G., Gonzalez, I., Gracia, Greeniaus, G., Greiner, W., Grichine, V., Grossheim, A., Guatelli, S., Gumplinger, P., Hamatsu, R., Hashimoto, K., Hasui, H., Heikkinen, A., Howard, A., Ivanchenko, V., Johnson, A., Jones, F. W., Kallenbach, J., Kanaya, N., Kawabata, M., Kawabata, Y., Kawaguti, M., Kelner, S., Kent, P., Kimura, A., Kodama, T., Kokoulin, R., Kossov, M., Kurashige, H., Lamanna, E., Lampen, T., Lara, V., Lefebure, V., Lei, F., Liendl, M., Lockman, W., Longo, F., Magni, S., Maire, M., Medernach, E., Minamimoto, K., Mora, Morita, Y., Murakami, K., Nagamatu, M., Nartallo, R., Nieminen, P., Nishimura, T., Ohtsubo, K., Okamura, M., O'Neale, S., Oohata, Y., Paech, K., Perl, J., Pfeiffer, A., Pia, M. G., Ranjard, F., Rybin, A., Sadilov, S., Salvo, E. D., Santin, G., Sasaki, T., Savvas, N., Sawada, Y., Scherer, S., Sei, S., Sirotenko, V., Smith, D., Starkov, N., Stoecker, H., Sulkimo, J., Takahata, M., Tanaka, S., Tcherniaev, E., Safai, Tropeano, M., Truscott, P., Uno, H., Urban, L., Urban, P., Verderi, M., Walkden, A., Wander, W., Weber, H., Wellisch, J. P., Wenaus, T., Williams, D. C., Wright, D., Yamada, T., Yoshida, H. & Zschiesche, D. (2003), 'G4–a simulation toolkit', Nuclear Instruments and Methods in Physics Research Section A:

Accelerators, Spectrometers, Detectors and Associated Equipment **506** (3), 250 – 303.

Ajzenberg-Selove, F. & Lauritsen, T. (1968), 'Energy levels of light nuclei (vii). A = 11-12', Nuclear Physics A **114** (1), 1 – 142.

Akhiezer, A. & Berestetskii, V. (1965), Quantum electrodynamics, Wiley-Interscience, New York.

Arce, P., Banerjeeb, S., Gonzleza, I., Klemc, J. & Nikitenkod, A. (1999), Detector Description of CMS using Geant4: CMS internal Note.

Auslender, V., Nekhaev, V., Panlov, A. & Tuvik, A. (1999), 'Compact ilu-type electron accelerators as a base for industrial 4-sided irradiation systems for cable and tubes', Radiation Physics and Chemistry **54**, 609–618.

Ballestrero, S., Bornman, F., Cafferty, L., Caveney, R., Connell, S., Cook, M., Dalton, M., Gopal, H., Ivesc, N., Lee, C., Mampe, W., Phoku, M., Roodt, A., Sibande, W., Sellschop, J., Topkin, J. & Unwuchola, D. (2009), Mineral-PET : Kimberlite sorting by nuclear-medical technology, in 'Proceedings of the 12th International Conference On Nuclear Reaction Mechanisms', Vol. 2, pp. 589–602.

Ballestrero, S., Connell, S., Caveney, R., Chapman, J., Korir, K., Sibiya, T., Raphotle, M., Fischer, C. & Rebuli, D. (2005), 'Feasibility study for the pit project'. (An internal document, not published).

Barber, W. C., George, W. D. & Reagan, D. D. (1955), 'Absolute Cross Section for the Reaction $C^{12}(\gamma, n)C^{11}$', Physical Review **98**, 73–76.

Behrens, H., Kobelt, M., Szybisz, L. & Thies, W.-G. (1975), 'On the ^{11}c $\rightarrow ^{11}$b β^+ transition', Nuclear Physics A **246** (2), 317 – 322.

Blasse, G. (1994), 'Scintillator materials', Chemistry of Materials **6** (9), 1465–1475.

Bocheck, G., Kulibaba, V., Ovcinnik, N. & Shramenko, B. (1998), '1.2 gev electron radiation spectra in thick tungsten single crystal and total radiation losses in tungsten, germanium and silicone single crystals', Nuclear Instruments and Methods in Physics Research .

Brown, B., Smallwood, R., Barber, D., Lawford, P. & Hose, D. (1999), Medical Physics and Biomedical Engineering, Institute of Physics Publishing, Bristol.

Cember, H. (1996), Introduction to Health Physics, 3rd edn, Wiley.

Chinaka, E., van Rooyen J., Zibi, Z. & Connell, S. (2012), 'Radiation shielding analysis and optimisation for the mineral-PET kimberlite sorting facility using a Monte Carlo code, MCNPX', available on-line at http://events.saip.org.za/getFile.py/access?contibId =10 &session=15&resId=0&materialId=paper&confId=14. cited on 11 Apr 2013.

Colsher, J. (1980), 'Fully-three-dimensional positron emission tomography', Physics in Medicine and Biology **25**, 103–115.

Cook, B. C., Baglin, J. E., Bradford, J. N. & Griffin, J. E. (1966), '$C^{12}(\gamma, n)C^{11}$ Cross Section to 65 MeV', Physical Review **143**, 724–729.

Daniel Ben, R., Deuther-Conrad, W., Scheuneman, M., Steinbach, J., Brust, P. & Mishani, E. (2008), 'Carborn-11 labeled indolylpropylamine analogue as a new potential PET agent for imaging of the serotonin transporter', Bioorganic & Medicinal Chemistry .

Dirac, P. (1930), On the annihilation of electrons and protons, in 'Mathematical proceedings of the Cambridge Philosophical Society', Vol. 26 , Cambridge University Press, pp. 361–375.

Dovbnya, A., Nikiforof, V. & Uvarov, V. (2005), 'Modeling and optimization of electron linac exit systems for nuclear technologies', Bulletin London Mathematical Society pp. 199–201.

Dove, E. (2003), 'Physics of medical imaging an introduction', Biomedical Engineering .

Enge, H. (1970), Introduction to nuclear physics, Edison-Wesley: London.

Eshwarappaa, K., Sanjeev, G., Siddappa, K., Kashyap, Y., Sinha, A., Sakar, P. & Godwal, B. (2007), 'Comparison of photoneutron yield from beryllium irradiated with bremsstrahlung next term radiation of different peak energy', Annals of Nuclear Energy .

Farr, R. & Allisy Roberts, P. (2006), Physics For Medical Imaging, Elsevier India P Ltd.

Ferbel, T. (1987), Experimental Techniques in High Energy Physics, Addison-Wesley, Menlo Park,California.

Ferguson, C. (2000), General purpose Source Particle Module for Geant4/SPARSET: Technical Note, UoS-GSPM-Tech. available on-line at http://geant4.cern.ch/support/about .shtml/ cited on 3 Dec 2007.

Fultz, S., Caldwell, J., Berman, B., Bramblett, R. & Harvey, R. (1966), 'Photoneutron cross sections for c^{12} and al^{27}', Physical Review **143** (3), 790–794.

Geani, S. & Geneva, C. (1998), 'Geant 4: An object-oriented toolkit for simulation in HEP', CERN/LHCC pp. 98–44. available on-line at http://geant4.web.cern.ch/geant4/.

Grichine, V., Bagulya, A., Lebedev, P., Marie, M., Urban, L., Giani, S. & Apostolakis, J. (2000), 'An implementation of ionisation energy loss in very thin absorbers for the GEANT4 simulation package', Nuclear Instruments and Methods, section A . also available on-line at http://geant4.web.cern.ch/geant4/results/publications.shtml.

Groom, D. (2004), Atomic and Nuclear Properties of Materials for 292 substances. available on-line at http://pdg.lbl.gov/2005/AtomicNuclearProperties/ cited on 29 Aug 2007.

Hake, H. & Wolf, H. (1996), The physics of Atom and Quanta, 5th edn, Springer-Verlag:Berlin.

Hamamatsu Photonics, K. K. (2001), 'Hamamatsu R2486 position-sensitive photomultiplier tubes with crossed wire anodes', Specications and Information Sheet .

Hammersley, J. & Handscomb, D. (1964), Monte Carlo Methods, Methuen:London.

Hendee, W. (1970), Medical Radiation Physics, Year Book Medical Publishers,Inc:Chicago.

Herzog, H. (2007), Methods and applications of positron-based medical imaging, in 'Proceedings of the 8th International Workshop on Positron and Positronium Chemistry', Vol. 76, pp. 337–342.

Hodgson, P., Gadioli, E. & Gadioli, E. E. (1997), Introductory nuclear physics, Oxford University press.

Hoffman, E., Huang, S. & Phelps, M. (1981), 'Quantitation in positron emission computed-tomography .4. effects of accidental coincidences', Journal of Computer Assisted Tomography **5**, 391–400.

IAEA (2000), 'IAEA photonuclear data library-cross sections and spectra up to 140 MeV', Bulletin London Mathematical Society **17**, 305–317.

Kawatsu, C. & Shevin, M. (2003), 'Parameters for the hot giant dipole resonance', Atomic Data and Nuclear Data Tales .

Knoll, G. (2000), Radiation Detection and Measurement, McGraw-Hill.

Krane, K. (1988), Introductory Nuclear Physics, John Wiley & sons:Canada.

Lecoq, P. (1998), 'Spin-off from particle detectors in the field of medicine and biology', Nuclear Instruments and Methods in Physics Research pp. 146–149.

Leo, W. (1994), Techniques for Nuclear and Particle Physics experiments, A how to approach, 2nd edn, Spriger-Verlag: New York.

Levin, C.S., H. E. (1999), 'Calculation of positron range and its effect on the fundamental limit of positron emission tomography system spatial resolution', Physics in Medicine and Biology **44**, 781–799.

Lochstet, W. & Stephens, W. (1966), '$^{12}c(\gamma,\ n)^{11}c$ giant resonance with gamma rays', Phys. Rev. **141** (3), 1002–1006.

Meyer, M. (1988), Natural Diamond, Handbook of industrial diamonds and diamond films, CRC Press, chapter 10.

Ollinger, J. & Fessler, J. (1997), 'Positron emission tomography', IEEE Signal Processing Magazine **14** (1), 43–55.

Pain, F., Dhenam, M., Gurden, H., Router, A., Lefebvre, F., Mastrippolito, R. & Laniece, P. (2008), 'A method based on Monte Carlo simulations and voxelized anatomical atlases to evaluate and correct uncertainties on radiotracer accumulation quantization in beta microprobe studies in the rat brain', Physics in Medicine and Biology **53**, 5385–5404.

Palmer, M. & Parker, J. (2004), 'High resolution imaging with positron emitters: modeling range blurring effects', Nuclear Science Symposium Conference Record, 2004 IEEE **5**, 2682–2685.

Phelps, M., Hoffman, E. & Mullani, N. (1975), 'Application of annihilation coincidence detection to transaxial reconstruction tomography', Journal of Nuclear Medicine **16** (3), 210–224.

Price, W. (1967), Nuclear Radiation Detection, 2nd edn, McGraw-Hill, New York.

Sellschop, J. & Connell, S. (2005), 'SA patent: Detection of diamonds'. ZA 2004/2010, 2006/08025.

Shapiro, J. (2002), Radiation Protection: A Guide for Scientists, Regulators, and Physicians, Editorial UPR.

Sorenson, J., Cherry, S. & Phelps, M. (1987), Physics in Nuclear Medicine, 3rd edn, London.

Sweet, W. & Brownell, G. (1953), 'Localization of brain tumors with positron emitters', Nucleonics **11**, 40–45.

Ter-Pogossian, M. & Phelps, M. (1975), Positron-emission transaxial tomograph for nuclear imaging (pett), in 'scientific assembly and annual meeting of the Radiological Society of North America', Vol. 114 of 60, Washington University: St. Louis, Chicago,IL, pp. 89–98.

Vertes, P. (2001), Test Calculations with IAEA Photonuclear Data Library, IAEA Nuclear Data Section, Wagramer Strasse-VIENA.

Wolf, A. & Redvanly, C. (1977), 'Carbon-11 and radiopharmaceuticals', International Journal of Applied Radiation and Isotopes **28**, 29–48.

Wong, C. (1954), 'Beta decay of f^{17} and c^{11}', Physical Review **95** (3), 765–766.

Yamamoto, M. (1981), 'Detector arrangement and sampling characteristics in rotary positron-emission computed-tomography', Physics in Medicine and Biology **26**, 489–499.